RESEARCH ARTICLE

Folylpolyglutamate synthetase mRNA G-quadruplexes regulate its cell protrusion localization and enhance a cancer cell invasive phenotype upon folate repletion

Michal Stark[1], May Levin[1,2], Igor Ulitsky[3] and Yehuda G. Assaraf[1]*

Abstract

Background Folates are crucial for the biosynthesis of nucleotides and amino acids, essential for cell proliferation and development. Folate deficiency induces DNA damage, developmental defects, and tumorigenicity. The obligatory enzyme folylpolyglutamate synthetase (FPGS) mediates intracellular folate retention via cytosolic and mitochondrial folate polyglutamylation. Our previous paper demonstrated the association of the cytosolic FPGS (cFPGS) with the cytoskeleton and various cell protrusion proteins. Based on these recent findings, the aim of the current study was to investigate the potential role of cFPGS at cell protrusions.

Results Here we uncovered a central role for two G-quadruplex (GQ) motifs in the 3′UTR of FPGS mediating the localization of cFPGS mRNA and protein at cell protrusions. Using the MBSV6-loop reporter system and fluorescence microscopy, we demonstrate that following folate deprivation, cFPGS mRNA is retained in the endoplasmic reticulum, whereas upon 15 min of folate repletion, this mRNA is rapidly translocated to cell protrusions in a 3′UTR- and actin-dependent manner. The actin dependency of this folate-induced mRNA translocation is shown by treatment with Latrunculin B and inhibitors of the Ras homolog family member A (RhoA) pathway. Upon folate repletion, the FPGS 3′UTR GQs induce an amoeboid/mesenchymal hybrid cell phenotype during migration and invasion through a collagen gel matrix. Targeted disruption of the 3′UTR GQ motifs by introducing point mutations or masking them by antisense oligonucleotides abrogated cell protrusion targeting of cFPGS mRNA.

Conclusions Collectively, the GQ motifs within the 3′UTR of FPGS regulate its transcript and protein localization at cell protrusions in response to a folate cue, inducing cancer cell invasive phenotype. These novel findings suggest that the 3′UTR GQ motifs of FPGS constitute an attractive druggable target aimed at inhibition of cancer invasion and metastasis.

Keywords Folylpolyglutamate synthetase, 3′UTR, G-quadruplex, Folic acid, RNA transport, Cell protrusions, Invasion

*Correspondence:
Yehuda G. Assaraf
assaraf@technion.ac.il
[1] The Fred Wyszkowski Cancer Research Laboratory, Department of Biology, Technion-Israel Institute of Technology, 3200003 Haifa, Israel
[2] Present address: May Levin, MeMed Diagnostics Ltd, Tirat Carmel, Israel
[3] Department of Immunology and Regenerative Biology and Department of Molecular Neuroscience, Weizmann Institute of Science, 7610001 Rehovot, Israel

Background

Directional single-cell migration is an orchestrated process pivotal for development, establishment and maintenance of proper organization of multicellular organisms, immune response, and disease progression, including cancer cell migration and metastasis [1–4]. Among the major regulators of cell migration are members of the Rho family of small guanosine triphosphatases

(GTPases), primarily Ras homolog family member A (RhoA), Ras-related C3 botulinum toxin substrate 1 (Rac1), and cell division control protein 42 homolog (CDC42) [5–7]. These GTPases undergo carboxymethylation which is crucial for cell migration [8, 9], affecting protein activation [9, 10], protein half-life [11], and subcellular protein localization [10, 12].

Protein methylation requires S-adenosylmethionine (SAM, AdoMet) as the methyl donor [13]; this one carbon methyl unit originates from 5-methyl-tetrahydrofolate (5-CH$_3$-THF) [14, 15], which is the dominant circulating THF cofactor [16]. THF cofactors serve as one-carbon donors in a multitude of key biosynthetic processes such as the de novo biosynthesis of nucleotides and amino acids [14], one of which is L-methionine that is further converted into SAM.

Most eukaryotic cells are auxotrophic for folates [17]; thus, they must obtain folates from their diet through specified influx transport systems [18]. However, since folates can be rapidly exported out of cells, their intracellular retention absolutely relies on the unique enzyme folylpolyglutamate synthetase (FPGS) which is essential for their cellular homeostasis [19]. FPGS catalyzes the successive addition of glutamate residues to the γ-carboxyl group of folates, resulting in their polyglutamylation [20] and intracellular accumulation up to three orders of magnitude higher than in the blood [21, 22]. Hence, FPGS is vital for the proliferation of normal and malignant cells.

The FPGS gene is translated into two isoforms, differing by an N-terminal leader sequence which directs the enzyme to mitochondria [23, 24], where FPGS mediates the retention of necessary folates for glycine biosynthesis [24]. The shorter isoform, termed cytosolic FPGS (cFPGS), was considered as a soluble protein, pivotal for purine and pyrimidine nucleotide biosynthesis [25]. We have recently shown that cFPGS is associated with the cellular cytoskeletal network and intracellular membranes, allowing the regulated transport of cFPGS to locations of folate metabolism, including the sites of folate uptake at the plasma membrane, the nucleus, the outer mitochondrial membrane, and the ER [26]. While our previous study demonstrated microtubule-dependent transport of the cFPGS protein, we herein show the actin-dependent transport of the cFPGS mRNA to cell protrusions. This protrusion-localization of the cFPGS mRNA requires the presence of its 3′UTR, and in particular two G-quadruplex (GQ) motifs found therein.

In the latter respect, GQs are composed of 4 runs of three (GGG$_4$) or four (GGGG$_4$) adjacent guanines (G-tracts) which spontaneously self-organize into four-stranded DNA/RNA structures [27, 28]. Bioinformatic analyses suggested that 300,000 GQ motifs are present in the human genome [29]. Importantly, it has been shown that these GQ motifs are not randomly dispersed throughout the genome, but are rather densely distributed in many key regulatory regions [30], including replication origins [31], telomeres [32], promoters, as well as 5′ and 3′UTRs [33, 34]. It has been well established that GQs which are present in the 3′UTR of mRNAs can regulate the subcellular localization of these transcripts in certain cells like neurons [35, 36].

Low serum folate levels have been shown to be associated with increased tumorigenicity [37–41] and enhanced metastasis [41–43]. Invasiveness and metastasis may be induced in the search for folates via chemotactic mechanisms. In this respect, we herein uncovered that the 3′UTR of FPGS, the GQ motifs in particular, induce cell invasion in response to pulse folic acid (FA) repletion, suggesting a role in tumor progression, migration, and metastasis under low folate conditions in the tumor microenvironment. This suggests a role for FPGS, not only in intracellular folate retention and homeostasis, but also in folate sensing and chemotaxis, highlighting FPGS 3′UTR GQ motifs as an attractive druggable target for inhibition of cancer migration and invasion.

Results and discussion

G-quadruplex elements in the 3′UTR of FPGS mRNA are required for its translocation to cell protrusions

In our recent study [26], multiple actin binding/modulating proteins were identified by immunoprecipitation as cFPGS interactors, including cofilin 1 (CFL1), vinculin (VCL), fascin (FSCN1), cortactin (CTTN), IQ motif containing GTPase-activating protein 1 (IQGAP1), and talin-1 (TLN1). Actin was not identified as an interactor, although immunofluorescence (IF) microscopy did demonstrate the co-localization of cFPGS and actin on sub-membranous actin stretches. Since many of these proteins are components of the actin machinery that regulates the formation and stabilization of cell protrusions for migration (i.e., pseudopodia, filopodia) [5, 44] and invasion (i.e., invadopodia) [45, 46], we hypothesized that cFPGS might localize to said protrusions to sustain cell migration and invasion in response to specific cues. Given that various protrusion-localized proteins were shown to be locally translated at the cell edges following the transport of their mRNA [47], e.g., CFL1 [48], VCL [49], actin-related protein 2/3 complex (Arp2/3) [50], and β-actin [51], we set to explore whether this is also true for cFPGS. The primary element shown to govern cellular mRNA localization is the 3′UTR; this was shown extensively in neuronal cells [52–54] and for protrusion-localized proteins such as β-actin [55], CFL1 [48], RAB13 [56], and STAT3 [57, 58]. Hence, we utilized the well-established MBSV6-MCP reporter system [59] to determine

Stark *et al. BMC Biology*   (2023) 21:13

Page 3 of 23

the subcellular localization of cFPGS mRNA. To this end, the 3′UTR of FPGS was subcloned into the pRK5/ FLAG-cFPGS (F-cFPGS) expression vector [26] and the sequence of 24xMS2V6 loops was inserted therein, as detailed in the "Methods" section (Fig. 1A) to yield the desired F-MS2 construct. The point of insertion of the 24xMS2V6 loops was selected carefully, to avoid the disruption of any regulatory element in the 3′UTR (Fig. 1B).

To gain a qualitative proof of concept that cFPGS mRNA localizes at cell protrusions, we induced cell migration and pseudopodia formation by the routinely used method of serum starvation and repletion. F-MS2 and MS2-coat protein (MCP)-GFP co-transfected cells were grown over night in serum-free medium, after which they were incubated for 1.5 h in complete growth medium, fixed, and scanned using a confocal microscope. The subcellular localization of the exogenous cFPGS mRNA was monitored by following the green MCP-GFP fluorescence, and compared between cells that were grown under complete medium (Fig. 2A, B), serum-deprived (Fig. 2C, D), and serum-repleted (Fig. 2E, F) conditions. Actin staining was used to visualize the boundaries of the cells. In full growth medium, the F-MS2 mRNA was evenly distributed in the cells, with occasional high accumulation foci at cell protrusions

(Fig. 2A, arrows). Whereas under serum deprivation, cells displayed less protrusions as previously shown [60], and F-MS2 mRNA was absent from the cell periphery (Fig. 2C). In contrast, upon serum repletion, F-MS2 mRNA was transported and accumulated at the edges of the newly formed, serum-induced filopodia (Fig. 2E, arrows). Consistently, FPGS mRNA was previously found to be enriched in protrusions of highly metastatic hepatocellular carcinoma cells [58].

Following the demonstration of the possible regulated transport of cFPGS mRNA to cell protrusions, we set to identify the element(s) within the 3′UTR of FPGS that govern(s) this translocation. Previous studies implicated GQ sequences in the 3′UTR of various neuronal genes, as the binding elements for RNA binding proteins (RBPs), that allowed the regulated transport of mRNAs to neuronal projections [35, 61]. It is reasonable that the same mechanism exists in non-neuronal cells, as several RBPs that were identified as GQ-binding proteins (GQBPs) [62–64] also transport RNA molecules to protrusions of migrating cells, such as fragile X mental retardation protein 1 (FMRP/FMR1) [57], or are a component of ribonucleoprotein complexes transported to cell protrusions, such as the RNA helicase DEAD box protein 3, X isoform (DDX3) [65], and the oncogene fused in sarcoma (FUS)

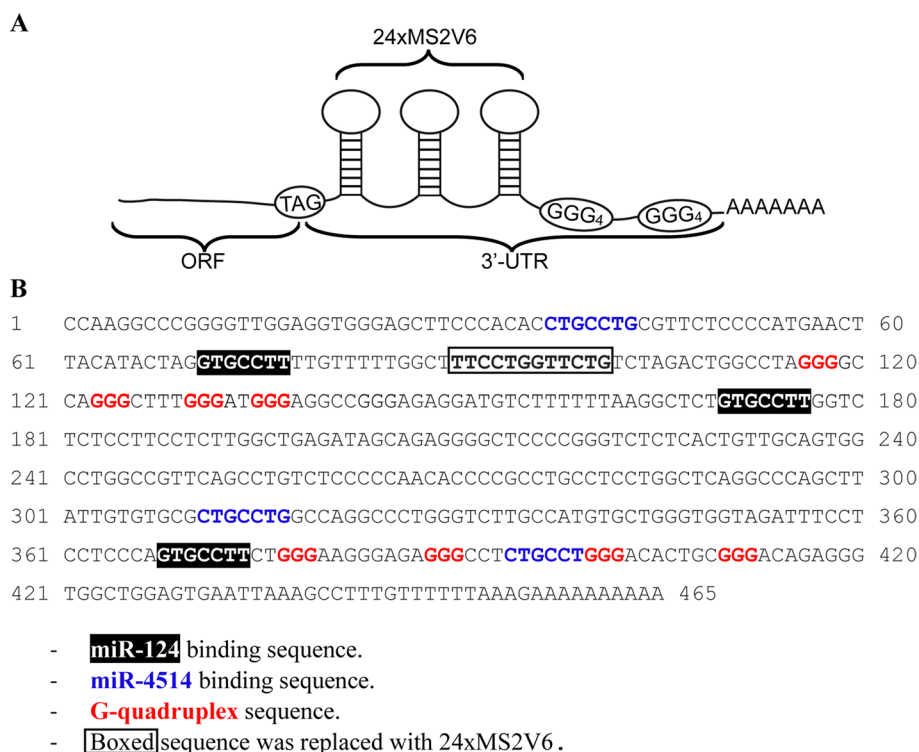**Fig. 1.** The 3′UTR of FPGS. **A** Schematic illustration of the 3′UTR and 24xMS2 sequences added to the FLAG-cFPGS expression vector. **B** Prediction of regulatory elements within the 3′UTR of FPGS and the insertion position of the 24xMS2 sequence
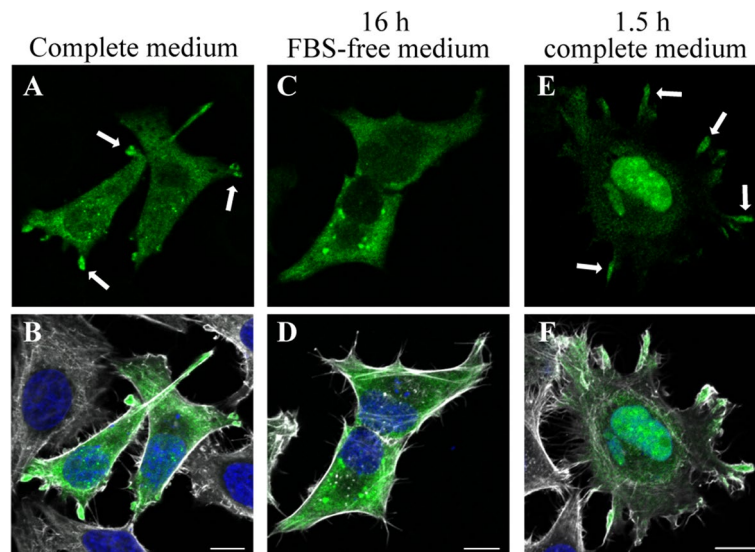
Stark *et al. BMC Biology*   (2023) 21:13

Page 4 of 23

Fig. 2. Confocal microscopy imaging of the subcellular localization of exogenous cFPGS mRNA harboring its native 3′UTR. HeLa cells co-transfected with FLAG-cFPGS-3′UTR-24xMS2 (F-MS2) and MCP-GFP were grown in full growth medium (**A**, **D**), serum-free medium (16 h, **B**, **E**), and serum-repleted medium (1.5 h, **C**, **F**). Fixed cells were stained with Hoechst 33342 (nuclei, blue fluorescence, 405 nm) and phalloidin (white, 630 nm) and were scanned using a confocal microscope (×63 magnitude). F-MS2 mRNA was detected by the green fluorescence of bound MCP-GFP (488 nm). Arrows point to cell protrusions with accumulated mRNA. Scale bars denote 10 μm. Shown are representative images of three independent experiments

[66]. Since the 3′UTR of FPGS is predicted to harbor two GQ sequences, we analyzed the 3′UTR of various protrusion-localized RNAs [48, 50, 56–58, 67–73] for the presence of GQ elements and compared their score to that of FPGS using the QGRS Mapper tool (Table 1). Although two-quartet GQs (i.e., GG_4) have been recently identified and shown to form secondary structures [74–76], they have yet to be implicated in RNA transport and have low prediction scores; hence, we restricted the analyses to a minimum of three G runs (i.e., GGG_4) and a maximum GQ length of 45 bp. Although the functional importance of the GQ elements shown in Table 1 has not been experimentally validated, except for the GQ of CAMK2A [35, 77], the mRNAs of CAMK2A, CFL1, and STAT3 are dependent on their 3′UTR for transport to cell protrusions [48, 57, 72], and all three are binding substrates of FMRP [57, 78, 79]; the latter has been shown to bind the majority of its RNA substrates through a GQ element [36, 61, 62, 80]. The actin crosslinkers filamin A and B (FLNA and FLNB) [81] were also found among FMRP's binding substrates [82].

As evident from Table 1, the G-scores of the GQs of FPGS are comparable and even higher than those of CFL1, FLNA, FLNB, STAT3, and CAMK2A. Functional UTR GQs have been shown to be selectively constrained [33] and it has been suggested that universal selection for GQ formation in the UTRs of eukaryotic genomes may be related to the biological functions of GQs [83].

Indeed, an initial examination of the 3′UTR sequences of FPGS orthologs suggests that the GQ motifs are conserved around the same position in Mammalia, and even in Lepidosauria (Additional file 1: Table S1). In order to evaluate the conservation of the GQs in FPGS 3′UTR during vertebrate evolution, we obtained the 3′UTR sequences of FPGS homologs from diverse vertebrate species from the RefSeq database and analyzed them using QGRS mapper to predict the top two scoring GQs. To test whether the predicted GQs were a reflection of the G/C content of the 3′UTR or a specific preference for GQ-forming sequences, we further compared the real 3′UTR sequences to sequences with the same composition that were randomly shuffled. Comparison of the QGRS mapping scores has shown that the FPGS 3′UTR had a significantly strong preference to form two non-overlapping GQs than expected by chance in most amniote species (Additional file 2: Figure S1). In most cases, the top two scoring GQs also had a better score than that predicted by chance in the sequences with the same nucleotide composition. This shows that the sequence in amniotes evolved under conditions that preferentially retain the potential to form two distinct GQs, likely due to their functional roles in subcellular RNA localization. Collectively, these data suggest that the FPGS 3′UTR GQ sequences should be considered functional regulatory elements.

Stark *et al. BMC Biology* (2023) 21:13

Page 5 of 23

Table 1 G-quadruplex sequences found by QGRS Mapper in the 3′UTR of cell protrusion-localized RNAs

Gene	Accession	Position[a]	Length	QGs	G-score	Ref[b]
FPGS	NM_004957	116	22	GGGGCCAGGGCTTTGGGATGGG	70	58, current
		377	36	GGGAAGGGAGAGGGCCTCTGCCTGGGACACTGCGGG	70	
CFL1	NM_005507	89	29	GGGCTGGGGGGATCCCAGCAGGGGGAGGG	66	48, 58, 69
FSCN1	NM_003088	339	28	GGGACGGTTGGGGGCTGGGAGCCCTGGG	70	58, 70
		493	23	GGGAAGGGAAGCTGTCGGGTGGG	65	
		670	19	GGGCGGGTAGGGGTGTGGG	70	
FLNA	NM_001456	233	20	GGGAGGGGTGAGGGATGGGG	71	58, 69
FLNB	NM_001457	1028	44	GGGTCTTTGGCCTGAAAGTTGGGAATGGTTGGGGGGAGAGAAGGG	62	58, 69
RAB13	NM_002870	57	40	GGGAGTGAGCAGGGGAGAAATAGCAGAGGGGCTTGGAGGG	67	56, 69, 71, 72
ACTR2	NM_005722	399	29	GGGATGGGGGGTGGTTCGGGATGGGTGGG	71	50, 70, 73
		564	33	GGGTTTTGTTGCGGGGGGGGAGGGTAACAATGGG	68	
		1819	39	GGGCCCGTACCTACTGGCAGTTGGGTTCAGGGAAATGGG	57	
ARPC4	NM_005718	96	20	GGGAGTTGGGTTGGGGTGGG	70	69, 72
		626	44	GGGGCCCAAAAGCCGGGCAACCTCTGGCTACAGGGGCCATTGGG	63	
STAT3	NM_139276	248	28	GGGGATGTGGCGGGGGGGTGGCTAGAGGG	64	57, 58
		1989	43	GGGCTTACCATTGGGTTTAAATCATAGGGACCTAGGGCGAGGG	70	
CAMK2A	NM_015981	335	37	GGGCTGGTGCCCACCAGGGGCTGGGGAGAAGGAGGGG	63	67, 68
		886	39	GGGTCAGGTTGGAAGGGGTGTAGGAAGAGGGGTGAGGGG	66	
		2674	39	GGGTGGGCAGCCACCTGGTGCCACCACAGGGCACCAGGG	52	
		3134	30	GGGGGGGGCGGGTGGGATGGGAAGAAGGGG	72	
CAPZB	NM_004930	453	26	GGGGTTGGGGGTCGTGGGGACAGGGG	107	58, 70, 72
		547	20	GGGGTGGGGGCTGGGGGGGGG	106	

FPGS folylpolyglutamate synthase, *CFL1* cofilin 1, *FSCN1* fascin, *FLNA* filamin A, *FLNB* filamin B, *RAB13* Ras-related protein Rab-13, *ACTR2* actin-related protein 2, *ARPC4* actin-related protein 2/3 complex subunit 4, *STAT3* signal transducer and activator of transcription 3, *CAMK2A* calcium/calmodulin-dependent protein kinase type II subunit alpha, *CAPZB* F-actin-capping protein subunit beta

[a] Nucleotide position within the 3′UTR

[b] Reference papers demonstrating the protrusion localization/enrichment of each RNA

To explore the possible contribution of these GQ elements to the transport of cFPGS mRNA to cell protrusions, we mutated each element separately on the F-MS2 expression vector and repeated the fetal bovine serum (FBS)-induction assay. Herein, we used IF microscopy to visualize the cell's boundaries with filamentous actin (F-actin) along with the cFPGS protein. As depicted in Fig. 3, the disruption of each GQ was sufficient to abrogate the transport of FPGS mRNA to cell protrusions upon serum repletion. The mRNA appeared to be retained in the cell body, presumably in the ER area (Fig. 3 F and K); this coincides with our previous hypothesis, suggesting that cFPGS is translated and transported through the ER-Golgi network [26]. Each of the two GQ elements appears to have a pivotal role in the subcellular transport of FPGS mRNA. This implies either of the following: (1) a cooperative binding of the GQs by two RBPs [84], (2) the two GQs oligomerize to a higher order structure which is bound/stabilized by an RBP [85–87], or (3) binding of the two GQs by a single RBP harboring multiple binding sites, resulting in 3′UTR bending [88, 89]. To ensure complete abolishment of cFPGS mRNA transport,

we generated a double GQ mutant (F-MS2-dmGQ) and used this construct upon subsequent experiments. Interestingly, the exogenous cFPGS protein (detected by an anti-FLAG antibody) colocalized with its cognate mRNA (Fig. 3 D, I, N), suggesting the localized translation of cFPGS, as was shown for various protrusion-localized proteins [68, 90].

cFPGS mRNA transport to cell protrusions is induced upon FA repletion and is GQ- and F-actin-dependent

FPGS is a key regulator of intracellular folate retention and homeostasis [19] and FA is a known chemoattractant [91–94] crucial for the migration and invasion of A549 non-small cell lung cells [10] as well as prostate cancer cells [95]. Moreover, a 24-h FA deprivation in HeLa cells consistently resulted in an increase in both migration and invasion [96]. Based on these findings, we explored the subcellular localization of cFPGS mRNA upon FA repletion. To this end, HeLa cells were deprived of FA for 14 days; on day 13, cells were transfected with F-MS2 and studied the next day by live fluorescence microscopy
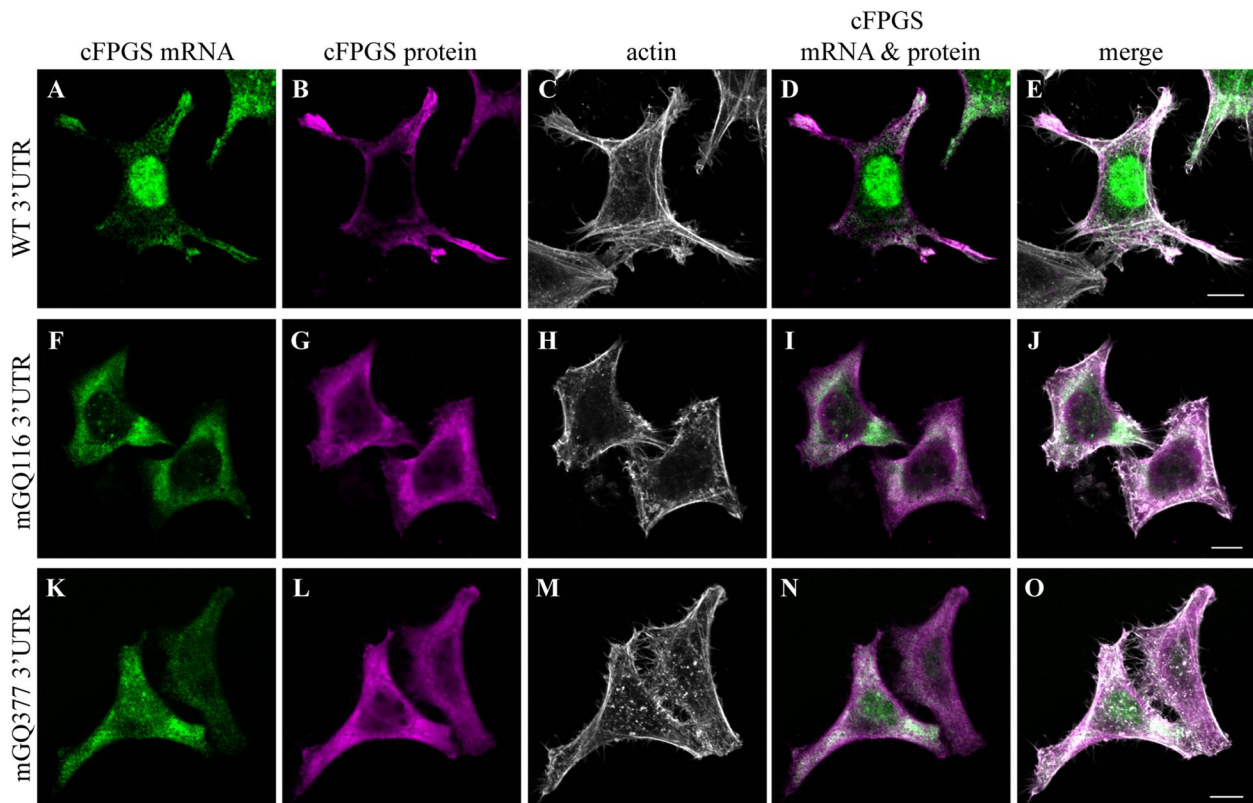
Stark *et al. BMC Biology*   (2023) 21:13

Page 6 of 23

Fig. 3. Disruption of the GQ elements at the 3′UTR of cFPGS mRNA abolishes its transport to cell protrusions. HeLa cells were co-transfected with MCP-GFP and FLAG-cFPGS-3′UTR-24xMS2 (F-MS2) harboring either the WT UTR (**A**–**E**), a mutated GQ at position 116 (mGQ116, **F**–**J**), or a mutated GQ at position 377 (mGQ377, **K**–**O**). Following 16 h of serum deprivation, cells were supplemented with complete growth medium for 1.5 h, fixed and subjected to IF microscopy. The localization of F-MS2 mRNA is indicated by MCP-GFP (green fluorescence, 488 nm), FLAG-cFPGS protein was detected by an anti-FLAG antibody (magenta, 405 nm), and F-actin was stained by DyLight 650 Phalloidin (white, 630 nm). Cells were scanned using a confocal microscope (×63 magnitude). The scale bars denote 10 μm. Shown are representative images of three independent experiments

imaging before and after the addition of 2 μM FA. Figure 4A depicts examples of individual cells, at different time points following FA addition, where cFPGS mRNA accumulation coincided with the elongation of a cell protrusion (Fig. 4A, top) or occurred in preexisting protrusions (Fig. 4A bottom). RNA accumulation at cell protrusions was most apparent around ~15min, after which the accumulated mRNA became dispersed. The experiment was repeated with the use of the F-MS2-dmGQ construct (Fig. 4B), which resulted in the lack of cFPGS mRNA accumulation during the same time frame. We have therefore chosen to conduct further experiments using a 15-min FA repletion pulse.

Next, to be able to efficiently quantify the FA-dependent transport of cFPGS mRNA to cell protrusions, and to evaluate the requirement of the 3′UTR GQ elements to this transport, we performed IF microscopy. HeLa cells deprived of FA were co-transfected with MCP-GFP along with either F-MS2 or F-MS2-dmGQ and subjected to a FA repletion pulse, following which cells were fixed and reacted with an anti-FLAG antibody.

The results obtained with the FA pulse (Fig. 5) were identical to those after FBS repletion (Fig. 3). Fifty-three percent of cells harboring F-MS2 displayed protrusion-localized cFPGS mRNA following a FA pulse (Fig. 5F, P), compared to only 3.8% of F-MS2-dmGQ harboring cells (Fig. 5K, P), the same percentage as in FA-starved cells (i.e., 3.9%, Fig. 5A, P). To further corroborate these findings, we utilized antisense oligonucleotides (ASOs) against the FPGS 3′UTR GQs. ASOs have been recently utilized for sequence-specific inhibition of RNA GQ folding, thus reducing protein translation [97–99]. We here employed the same technique with the aim to abrogate the FA-induced cell protrusion localization of cFPGS mRNA. While the non-targeted ASO-Ctr had no effect on cFPGS mRNA localization following a 15-min FA-pulse repletion, each of the GQ-targeted ASOs alone reduced the percentage of cells with protrusion-localized mRNA by ~50% (Fig. 5Q). No further reduction was observed when both ASOs were used together, corroborating their cooperative role in cFPGS mRNA localization in response to FA repletion.
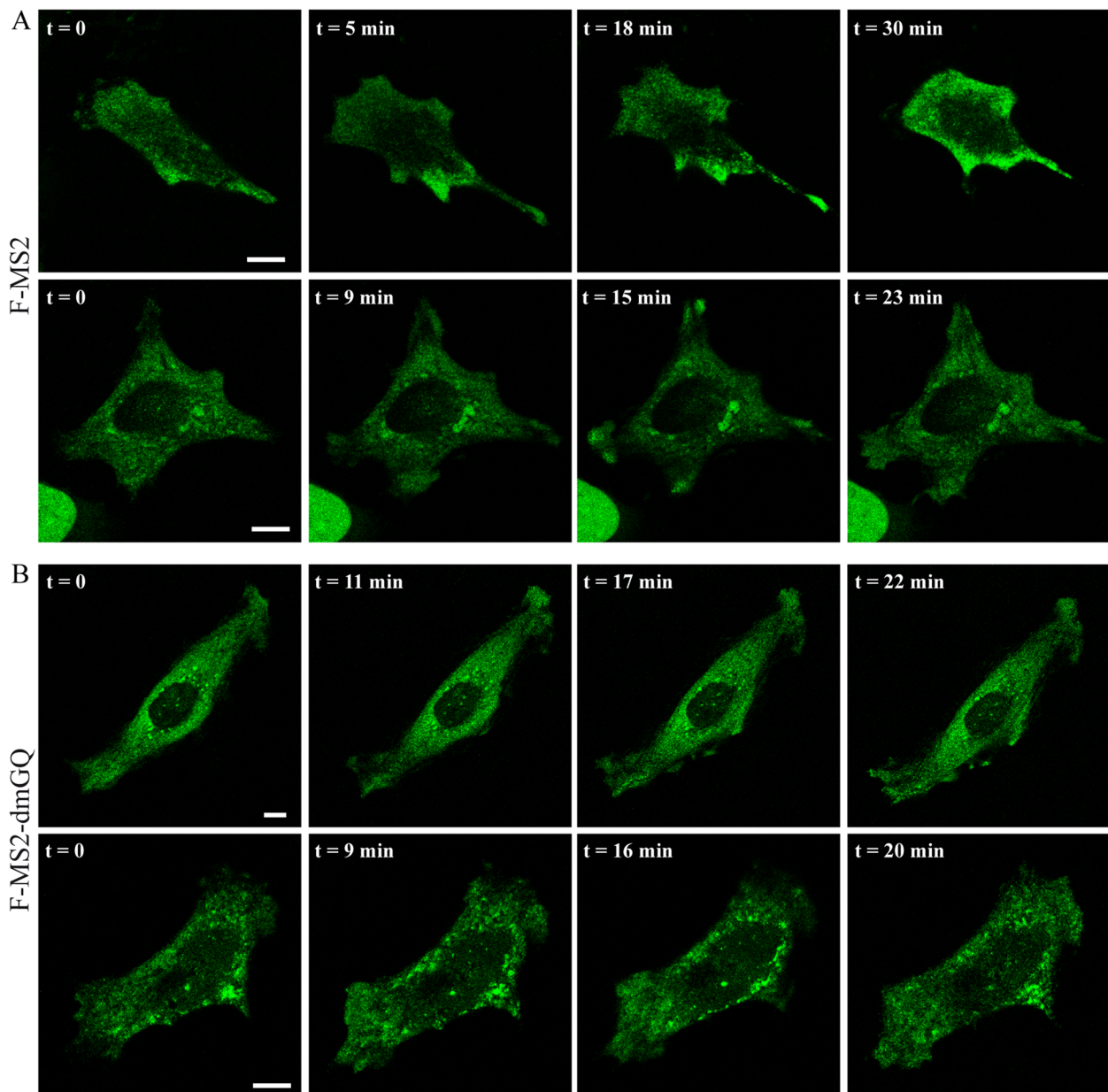
Stark *et al. BMC Biology*   (2023) 21:13

Page 7 of 23

Fig. 4. Time-lapse depiction of FA-induced cFPGS mRNA accumulation in a cell protrusion. HeLa cells deprived of FA for 13 days were co-transfected with MCP-GFP along with either F-MS2 (**A**) or F-MS2-dmGQ (**B**). The next day, the distribution of cFPGS mRNA (MCP-GFP, 488 nm) was monitored in single cells by live fluorescence imaging before ($t = 0$) and after the addition of 2μM FA to the growth medium. Cells were scanned with a confocal microscope (×63 magnitude). The scale bars denote 10 μm

Interestingly, upon FA repletion cells harboring the F-MS2-dmGQ construct (Figs. 3, 4, and 5) presented less protrusions per cell than cells harboring the F-MS2 construct. When comparing the two populations of cells (50 cells from each group), the average number of protrusions for the WT UTR was 7 ± 1.7 vs. 2.7 ± 1.2 for the dmGQ UTR ($p = 1.9 \times 10^{-26}$), suggesting a role for cFPGS mRNA in protrusion formation.

Out of the three most studied RBPs mediating the transport of mRNA to cell protrusions, i.e., FMRP [61, 79, 100]; adenomatous polyposis coli, APC [101–103]; and Zipcode binding protein 1, ZBP1 [104, 105], only FMRP recognizes and binds RNA GQs [61, 62, 106]. Since FMRP is dependent on microtubules for mRNA transport [107, 108], and as we have previously demonstrated the association of the cFPGS protein with the cellular
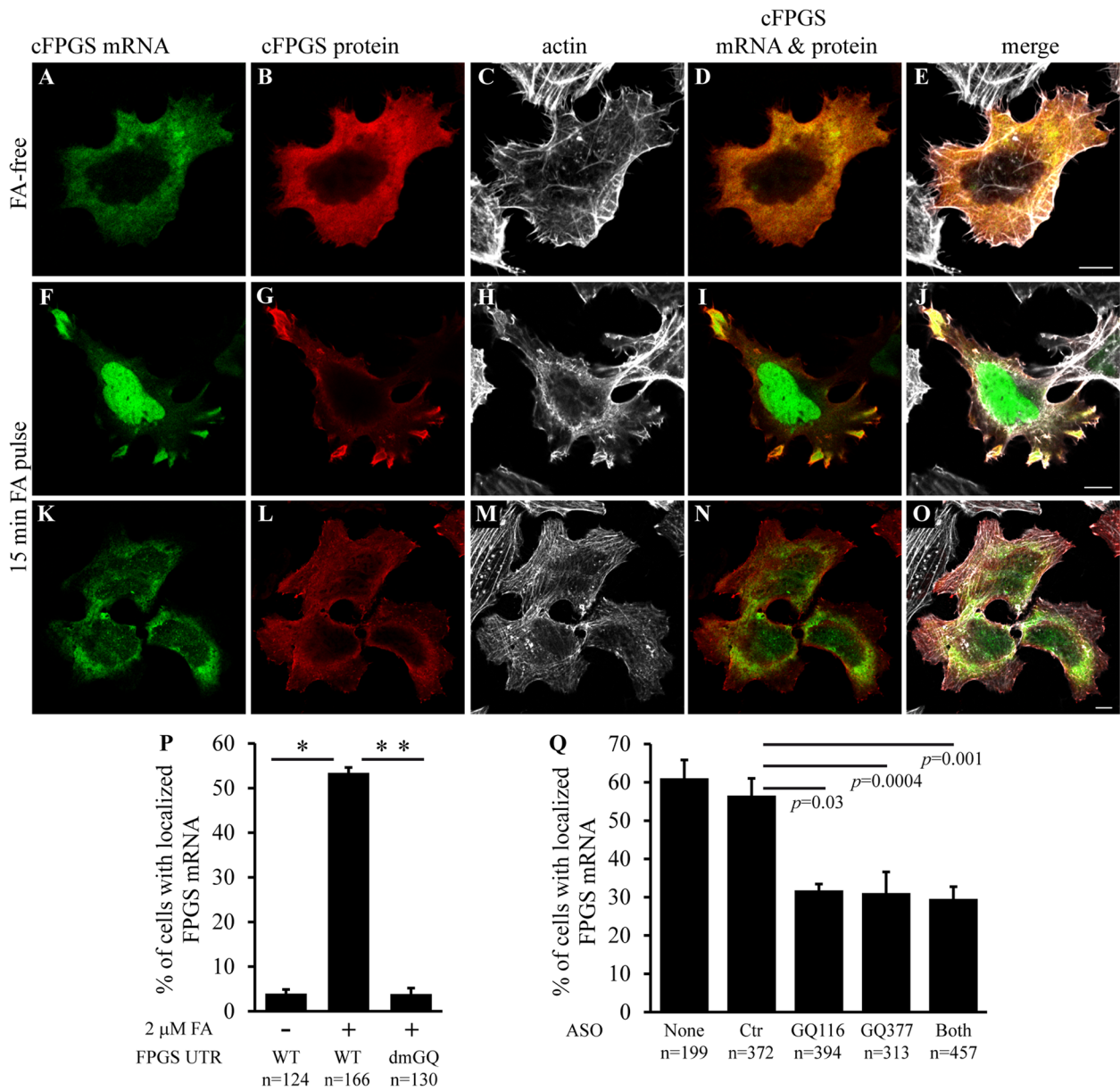
Fig. 5. The 3′UTR GQ elements are required for FA-induced cFPGS mRNA transport to cell protrusions. **A–P** On day 12 of FA deprivation, HeLa cells were co-transfected with MCP-GFP and F-MS2 (**A–J**) or F-MS2-dmGQ (**K–O**). Each transfection was divided into 2 wells and left to recover. At day 14, control cells remained FA-free (**A–E**) and the rest were subjected to a 15-min FA pulse (**F–O**), prior to fixation and IF microscopy. **Q** On day 13 of FA-deprivation, HeLa cells were co-transfected with MCP-GFP and F-MS2 along with ASOs as indicated. The next day, cells were subjected to a 15-min FA pulse, prior to fixation and microscopy. The localization of cFPGS mRNA was indicated by MCP-GFP (green, 488 nm), FLAG-cFPGS protein was detected by an anti-FLAG antibody (red, 543 nm), and F-actin was stained by DyLight 650 Phalloidin (white, 630 nm). Cells were scanned and manually counted using a confocal microscope (×63 magnitude). The scale bars denote 10 μm. **P, Q** Percentage of cells displaying protrusion-localized cFPGS mRNA. Shown are the mean percentage of cells ± S.D. from three independent experiments, *n* = total number of cells counted. *$p < 0.0006$, **$p < 0.00003$

cytoskeletal network, primarily with microtubules [26], we explored the dependence on microtubules for the FA-induced protrusion localization of cFPGS mRNA (Fig. 6). Following FA deprivation, transfected cells were pre-treated with the microtubule depolymerizing agent

vinblastine (VBT) [109] for 1 h before FA repletion; cells were then fixed and subjected to IF microscopy. Surprisingly, VBT did not hinder the accumulation of cFPGS mRNA and protein in cell protrusions (Fig. 6F–J). In fact, the percentage of cells with localized mRNA was greater
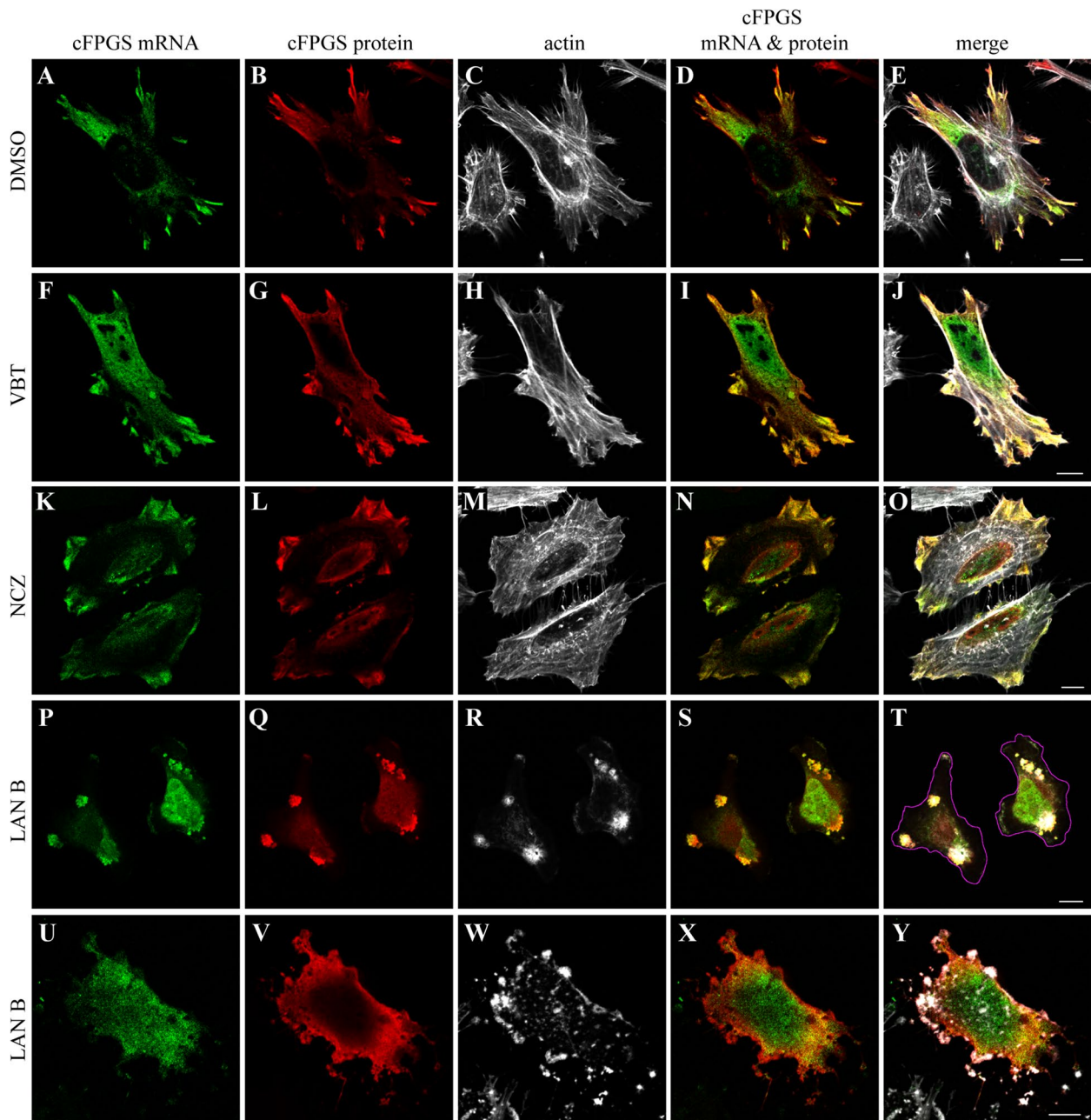
Stark *et al. BMC Biology*   (2023) 21:13

Page 9 of 23

Fig. 6. cFPGS mRNA transport to cell protrusions is dependent on actin filaments. HeLa cells, deprived of FA for 12 days, were co-transfected with MCP-GFP along with either F-MS2 (**A**–**T**) or F-MS2-dmGQ (**U**–**Y**). The next day, each cell group was split into different wells and left to grow in FA-free medium for an additional 24 h. Cells were pre-treated for 1 h with 0.1% DMSO (vehicle, **A**–**E**), 40 µM VBT (**F**–**J**), 10 µM NCZ (**K**–**O**), or 250 nM LAN B (**P**–**Y**) and supplemented with 2 µM FA for 15 min before fixation and IF microscopy. The localization of cFPGS mRNA is indicated by MCP-GFP (green fluorescence, 488 nm), FLAG-cFPGS protein was detected by an anti-FLAG antibody (red, 405 nm), and F-actin was stained by DyLight 650 Phalloidin (white, 630 nm). **T** The silhouette of the cells was outlined with a purple line. Cells were scanned using a confocal microscope (×63 magnitude). The scale bars denote 10 µm. Shown are representative images of three independent experiments

with the microtubule depolymerizing agent than in control cells (66.5% vs. 53.4% $p = 0.02$, $n = 140$ and 166 cells for Ctr and VBT, respectively). To verify that the microtubules were disrupted by VBT, cells were reacted with an anti-α-tubulin (α-Tub) antibody (Additional file 2: Figure S2). Indeed, following VBT treatment, microtubules appeared as short rod-like crystals as previously shown (Additional file 2: compare Figure S2L & Q to S2B & G)

[110, 111], while cFPGS protein accumulated in cell protrusions (Additional file 2: Figure S2K & P). The microtubule-independent transport of cFPGS mRNA was also confirmed with the microtubule dynamics disrupting agent nocodazole (NCZ) [112] (Fig. 6K–O).

The disruption of microtubules not only increased the percentage of cells with protrusion-localized cFPGS mRNA after a 15-min FA pulse, but also increased the residence time of said mRNA in protrusions. While drug-free cells exhibited mRNA dispersion after ~30 min (Fig. 3), with no cells harboring localized mRNA after 2 h (Additional file 2: Figure S3 A, C), VBT-treated cells retained the protrusion and the localized mRNA even after 3 h (Additional file 2: Figure S3, E, G). Previous studies demonstrated that filopodia remain intact and motile after disruption of microtubule with VBT and/or NCZ [113, 114]. Although many studies describe the transport of mRNA to cell protrusions, we could not find any publication describing the fate of mRNA after its local translation; does it undergo dispersion or degradation? Our current results suggest that while microtubules are not required for cFPGS mRNA transport to cell protrusions, they are required for mRNA retrograde transport/degradation.

As ZBP1 was shown to use actin filaments for RNA transport [51, 105], in addition to microtubule, we pretreated the cells with the actin polymerization inhibitor latrunculin B (LAN B) before FA-repletion (Fig. 6P–T). Under these inhibitory conditions, both cFPGS mRNA and protein co-localized with actin in large aggregates without reaching the cell edges. Since mutating the GQ elements in the FPGS 3′UTR disrupted mRNA transport to cell protrusions (Fig. 5), we hypothesized that it will abolish the physical connection between the mutated transcript and the actin cytoskeleton. Indeed, when cells were transfected with the MS2-dmGQ construct prior to LAN B treatment, cFPGS mRNA was distributed within the cells and not aggregated along with actin (Fig. 6U–Y). Moreover, the cFPGS protein, translated from the MS2-dmGQ construct, did not aggregate with actin as did the protein from the WT transcript (Fig. 6, compare V to Q), suggesting that cFPGS is not only locally translated at cell protrusions, as shown for many mRNAs [68], but is also translated while in transit, as was previously demonstrated [90].

As detailed in the "Methods" section, a point mutation resulting in a V525A substitution (V567 in the mitochondrial FPGS isoform) was introduced close to the C-terminus of cFPGS, to facilitate the subcloning of the 3′UTR into the pRK5 expression vector. When we performed IF microscopy with this V525A mutated construct, termed F-cFPGS-V525A, to ensure that the mutation did not interfere with the localization of the

cFPGS protein, we were surprised to find it in perinuclear vesicles (Additional file 2: Figure S4, A-D). This vesicular localization of cFPGS-V525A resembled that of the WT cFPGS which we previously reported, following treatment with LAN B and brefeldin A [26]. Based on our hypothesis that cFPGS translation and sorting occur through the ER-Golgi network [26], the V525A substitution might disrupt the ER export signal of cFPGS, as a single C-terminal valine was shown to operate as a strong ER export signal [115]. Consistently, previous findings revealed that a C-terminal valine is involved in the rapid and selective ER export of the FXYD7 protein, a regulator of Na^+/K^+ ATPase [116]. Indeed, cFPGS V525 which is located in a conserved hydrophobic patch, is completely conserved across eukaryotes, suggesting it is an essential residue. This substitution was corrected before further experiments were performed; however, since we had indications that cFPGS mRNA undergoes translation while in transit and/or protrusion-localized translation, the FLAG-cFPGS-V525A-3′UTR expression vector was used to explore this possibility. FA-depleted cells were transfected with said plasmid and used for IF microscopy before and after a pulse repletion with FA (Additional file 2: Figure S4). Under FA starvation, the cFPGS-V525A protein appeared in intracellular clusters (Additional file 2: Figure S4, E and K) which were juxtaposed to the ER marker calnexin (CANX) (Additional file 2: Figure S4, G, H and M). However, following a 15-min FA pulse, cFPGS-V525A assumed a dispersed localization and reached the cell periphery (Additional file 2: Figure S4, P and U, arrows). This suggests that following FA repletion, cFPGS-V525A was not retained in the ER since it was not translated therein. These results support both the ER as the first station for cFPGS mRNA and the regulation of its site of translation—either in the ER or cell protrusions.

FA-induced cFPGS mRNA transport to cell protrusions is dependent on the RhoA pathway

Actin-dependent RNA transport to cell protrusions is not very common and has been primarily studied with β-actin mRNA [117, 118], which is transported by the actin-dependent RBP ZBP1 [51, 105]. The dependence on actin for cFPGS mRNA transport is interesting, as the Krupenko group showed that the actin cytoskeleton is affected by dietary folates through the phosphorylation state of CFL1, i.e., folate deprivation results in decreased levels of inactive phosphorylated CFL1 (pCFL1) [10, 119]. Activated CFL1 depolymerizes and severs actin filaments, whereas pCFL1 dissociates from G/F actin as a result of reduced affinity [120]. The regulation of CFL1 phosphorylation is governed by a RhoA-dependent cascade [10, 121], whereas the localization and activation of RhoA is regulated by its methylation state [10, 122];

inactivated RhoA is anchored to the ER membrane via a prenyl moiety and is released upon prenylcysteine carboxymethylation [10]. FA, as a one-carbon unit donor in multiple cellular reactions, is required for SAM-dependent methylation [14, 123], and as such folate deprivation results in an ER-bound inactive RhoA [10]. The dependency of RhoA on carboxymethylation led Oleinik et. al. to conclude that RhoA is an immediate cellular sensor of FA status [10].

As β-actin mRNA delivery to cell protrusions was shown to be dependent on Rho-associated protein kinase (ROCK) and myosin II [117, 118], and since RhoA activity can be regulated by FA, it is plausible that RhoA senses the folate cue which initiates the transport of FPGS mRNA to the periphery. We utilized several inhibitors of the RhoA pathway to determine whether it is required for the transport of cFPGS mRNA to cell protrusions (Fig. 7A): Cysmethynil (CyMl) is a potent inhibitor of protein-S-isoprenylcysteine O-methyltransferase (ICMT) [124, 125] which carboxymethylates RhoA [122, 126] among other proteins. Y27632 is a *bona fide* inhibitor of the RhoA effectors ROCK 1/2 [127]. Blebbistatin (Blebb) is an inhibitor of the ATPase and gliding motility activities of myosin II [128, 129]. Treatment with any of these three inhibitors resulted in a significant reduction in the percentage of cells exhibiting cFPGS mRNA localization at cell protrusions upon FA repletion (Fig. 7B), indicating the importance of the RhoA pathway to FPGS mRNA transport to cell protrusions.

We propose a feedback loop between RhoA and cFPGS: Under FA deprivation, cFPGS is retained at the ER—from which it can be transported, in a microtubule-dependent rout, to intracellular locations of folate metabolism—where the FA sensor RhoA resides. Upon FA repletion and methylation of RhoA, it activates the pathway leading to cFPGS mRNA transport and translation at cell peripheries, where the FPGS enzyme—by rapid polyglutamylation—enables the accumulation of folates necessary for actin remodeling and cell migration.

The 3′UTR GQs of FPGS are required for a FA-induced cell invasion phenotype

To examine the validity of this putative feedback loop and explore the possible FA-dependent induction of an invasive phenotype, we utilized an inverted invasion assay [130, 131]. The following are the considerations for using this specific assay in which cells plated at the bottom of the well invade the top collagen (Col) matrix: (1) The widely used Boyden chamber Transwell invasion assay utilizes a commercially available basement membrane matrix, such as Matrigel or Cultrex, which consist of DMEM medium [132, 133]. DMEM contains ~9 µM FA, hence curtailing any assessment of FA-induced invasion potential. In contrast, the inverted invasion assay we utilized employs pure Col solubilized in acetic acid solution; this allows for the exogenous addition of a FA-containing medium on top of the FA-free collagen. (2) The basis for refraining from using the conventional Transwell system is the poor diffusion of medium components including FA from the bottom chamber with FA-containing medium into the upper Col matrix, precluding a FA-driven chemotactic effect and hence preventing any possibility of migration and invasion towards the Col matrix. The current inverted assay allows for the gravitational percolation of the growth medium into the Col gel sieve. As such, the bottom-plated cells can undergo an upwardly directed migration and invasion into the FA-containing Col in a chemotactic manner, as compared to a FA-free collagen. In traditional invasion assays, the Matrigel is supplemented with 1% FBS, thus allowing the cells to invade the growth factor-containing matrix and migrate close to the Transwell membrane where a micro-gradient of growth hormones induces the directional invasion of the cells to the underlaid growth medium containing 10% FBS. (3) The inverted invasion assay allows physical confinement where cell migration is dependent on the RhoA pathway [134, 135]. A concentration of 2.4 mg/ml type I collagen, used in this protocol, should generate a confined space with ~3-µm

(See figure on next page.)

Fig. 7. The RhoA-ROCK-Myosin II pathway is required for the transport of cFPGS mRNA to cell protrusions. HeLa cells, deprived of FA for 12 days, were co-transfected with MCP-GFP and F-MS2. The next day, transfected cells were split into 5 wells and left to grow in FA-free medium for an additional 24 h. Cells were pre-treated for 1 h with 0.1% DMSO (vehicle, **A**–**C**), 30 µM CyMl (**D**–**F**), 20 µM Y27632 (**G**–**I**), or 15 µM Blebb (**J**–**L**) and supplemented with 2 µM FA for 15 min before fixation and microscopy. The localization of cFPGS mRNA is indicated by MCP-GFP (green fluorescence, 488 nm) and F-actin is stained by DyLight 650 Phalloidin (white, 630 nm). Cells were scanned using a confocal microscope (×63 magnitude). The scale bars denote 10 µm. Shown are representative images of three independent experiments. **M** Confocal microscopy was used to count cells with protrusion-localized cFPGS mRNA. Shown are the mean percentage of cells ± S.D. from three independent experiments, *n* = total number of cells counted. All *p* values ≤ 0.001. Stop signs denote pharmacological inhibition detailed in **N**. **N** Illustration of the RhoA-ROCK-Myosin II pathway and the sites of pharmacological inhibition used (marked by a stop sign). RhoA is anchored to the ER membrane via a prenyl moiety and is retained therein under folate deprivation. Elevated levels of tetrahydrofolate cofactors increase the availability of S-adenosylmethionine (Me) leading to the carboxymethylation of RhoA by ICMT, which can be inhibited by CyMl. Following carboxymethylation RhoA is released from the ER and translocates to the plasma membrane, where it activates ROCK1/2; the latter can be inhibited by Y27632. ROCK activates myosin II by both phosphorylating the myosin light chain (MLC) and inhibiting the activity of MLC-phosphatase (MLCP). Myosin ATPase activity can be inhibited by Blebb

Stark *et al. BMC Biology* (2023) 21:13

Page 12 of 23
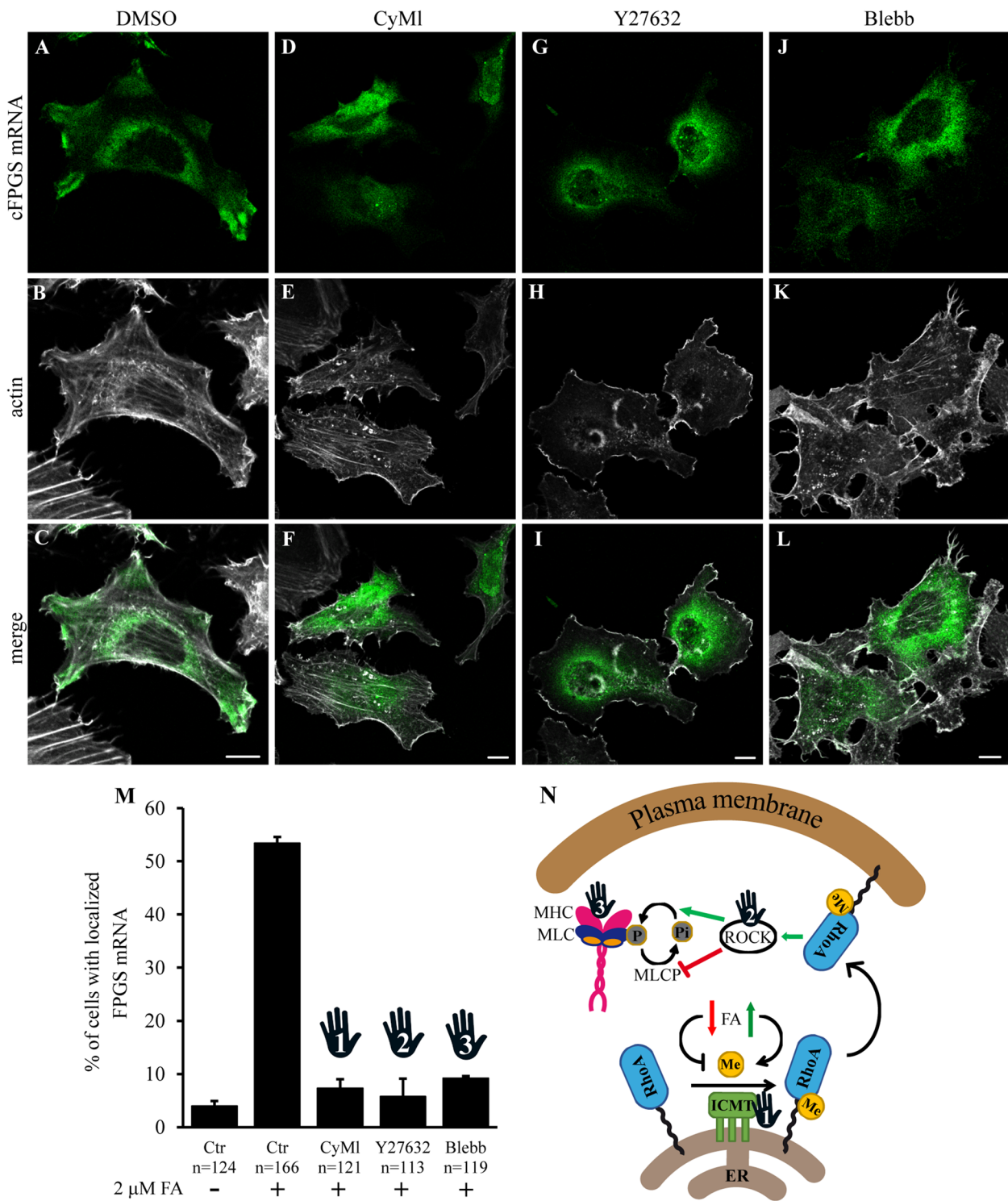
Fig. 7. (See legend on previous page.)

diameter pores [136–138]. Various cell lines, including HeLa, switch to a fast amoeboid migration phenotype, which includes the formation of a stable bleb [135, 139, 140]. FA-deprived cells were transfected separately with

a construct for either cFPGS without a 3′UTR (F-cFPGS), F-MS2, or F-MS2-dmGQ. Each construct was co-transfected with an expression vector harboring a fluorescent protein to allow monitoring by fluorescence microscopy,

i.e., F-cFPGS & BFP, F-MS2 & GFP, and F-MS2-dmGQ & RFP. Cells were mixed, seeded on glass plates, and overlaid with Col under three conditions: FA-containing Col immersed in FA-containing medium, FA-free Col immersed in FA-free medium, and FA-free Col immersed in FA-containing medium (Additional file 2: Figure S5). Cells were incubated for 40 h before they were visualized by live confocal imaging using focus stacking to record images at different focal planes (i.e., Z-stacks), allowing the generation of 3D images, and measure the spreading distance of each cell (Fig. 8 and Additional files 3, 4, 5, 6, 7, 8, 9, 10, 11: movies S1-S9).

When FA was present in the cells' immediate surroundings (i.e., within the Col), cells harboring F-cFPGS and F-MS2 developed a single bleb per cell, either from the cell body or from a protrusion, and the blebs developed in an upward direction, i.e., the leading edge (Fig. 8A, D, Additional file 3, 6: movies S1, S4). This is consistent with leader bleb-based migration [139, 141, 142], although the cells here were not round and maintained normal cell protrusions. Metastatic cancer cells were previously shown to have the ability to switch between protrusion types to optimize their migration in different environments [143, 144] and even exhibit an amoeboid/mesenchymal hybrid phenotype [145] under the control of RhoA [146]. Indeed, for cancer metastasis to occur, malignant cells must traverse a range of tissue environments with diverse physicochemical properties; this is accomplished, at least in part, by cells adjusting their migration mode to one that is best suited to the actual environment [147]. Blebs were shown to act as sites of extracellular matrix adhesion and re-organization during hybrid mode cell invasion [145]. In contrast, cells expressing F-MS2-dmGQ failed to develop any bleb (Fig. 8G, Additional file 9: movie S7). Each cell spanned ≤10 μm on the *Z* axis, excluding F-MS2-harboring cells which had very large blebs. Clearly, in the presence of FA, there was no need for the cells to spread out as FA was readily available. Under FA deprivation, the blebs were under the cells, following and not leading (Fig. 8B, E, H, Additional files 4, 7, 10: movies S2, S5, S8). This was the only condition under which some F-MS2-dmGQ harboring cells developed blebs (Fig. 8, compare H to G and I); however, they were relatively small. Interestingly,

while the blebs that were formed under the expression of F-MS2 seemed to have higher content density than the cell body (i.e., higher fluorescent intensity, Fig. 8E, Additional file 7: movie S5), the blebs that were formed in the other cells displayed very weak fluorescence, making them appear almost transparent (Fig. 8B, H, Additional files 4, 10: movies S2, S8), suggesting a different composition of these blebs resulting from uneven distribution of the cytosolic content between the cell body and the bleb. Interestingly, leading pseudopods of invading cells are characterized by a higher cell mass density [148]. In the pursuit of FA, cells spread a longer distance reaching ~20 μm, and yet the blebs were close to the cell body. The most significant changes in cellular behavior elicited by the three FPGS constructs were observed when FA was supplemented in the growth medium, slowly diffusing into the Col matrix as a vitamin chemoattractant. Cells expressing the UTR-null cFPGS transcript resembled those growing in the presence of FA, i.e., one upward-directed leader bleb per cell and short distance spreading (Fig. 8C, Additional file 5: movie S3). When the 3′UTR GQs were mutated, cells did not develop any blebs and cell spreading was < 10 μm (Fig. 8I, Additional file 11: Movie S9). In stark contrast, cells expressing FPGS with the WT UTR exhibited multiple blebs, with varying sizes, locations, and directions (Fig. 8F, Additional file 8: movie S6), with each cell spreading ≥15 μm. Additional file 2: Figure S6 allows to compare the morphology of cells harboring the WT UTR and dmGQ-UTR within the same growth area when FA-containing medium was added on top of the Col gel. FPGS WT-UTR, but not the dmGQ-UTR, induced the formation of leading blebs and invasion higher into the Col matrix. F-MS2 bearing cells developed protrusions from which blebs were formed and occasionally released (Fig. 8F, J, K, arrows); a string of vesicles formed at the tip of a cell protrusion (Fig. 8J) was released when a new bleb formed at said protrusion (Fig. 8K). Tumor cell blebbing and vesicle shedding are known phenomena that facilitate migration and invasion [149–151], specifically the very large oncosomes which contain matrix metalloproteinases, among others [152, 153].

A leader bleb can force its way forward by a net transfer of cytoplasm in the direction of migration [144], hence

(See figure on next page.)

Fig. 8. The 3′UTR of FPGS enhances cell migration under confined conditions. FA-deprived HeLa cells, co-transfected with either F-cFPGS (3′UTR-null) and BFP (**A**–**C**), F-MS2 and GFP (**D**–**F**, **J**, **K**), or F-MS2-dmGQ and RFP (**G**–**I**), were overlaid with FA-containing collagen and medium (**A**, **D**, **G**), FA-free collagen and medium (**B**, **E**, **H**), or FA-free collagen and FA-containing medium (**C**, **F**, **I**–**K**) as detailed in Figure S1. Following 40 h of incubation, cells were visualized by confocal microscopy using focus stacking (i.e., Z-stacks), and 3D semi-translucent images were generated. Each image is shown from both a bottom and top view, with a color gradient representing the depth within the image. **J**, **K** Images of the same cell with a 2.5-h interval, during which a string of vesicles detached from the cell protrusion, and a new bleb formed at the tip of the protrusion. Arrows point at vesicles released from cell protrusions. The scale bars denote 10 μm. Transition through the Z-stacks can be seen in the supplementary movies S1-S9
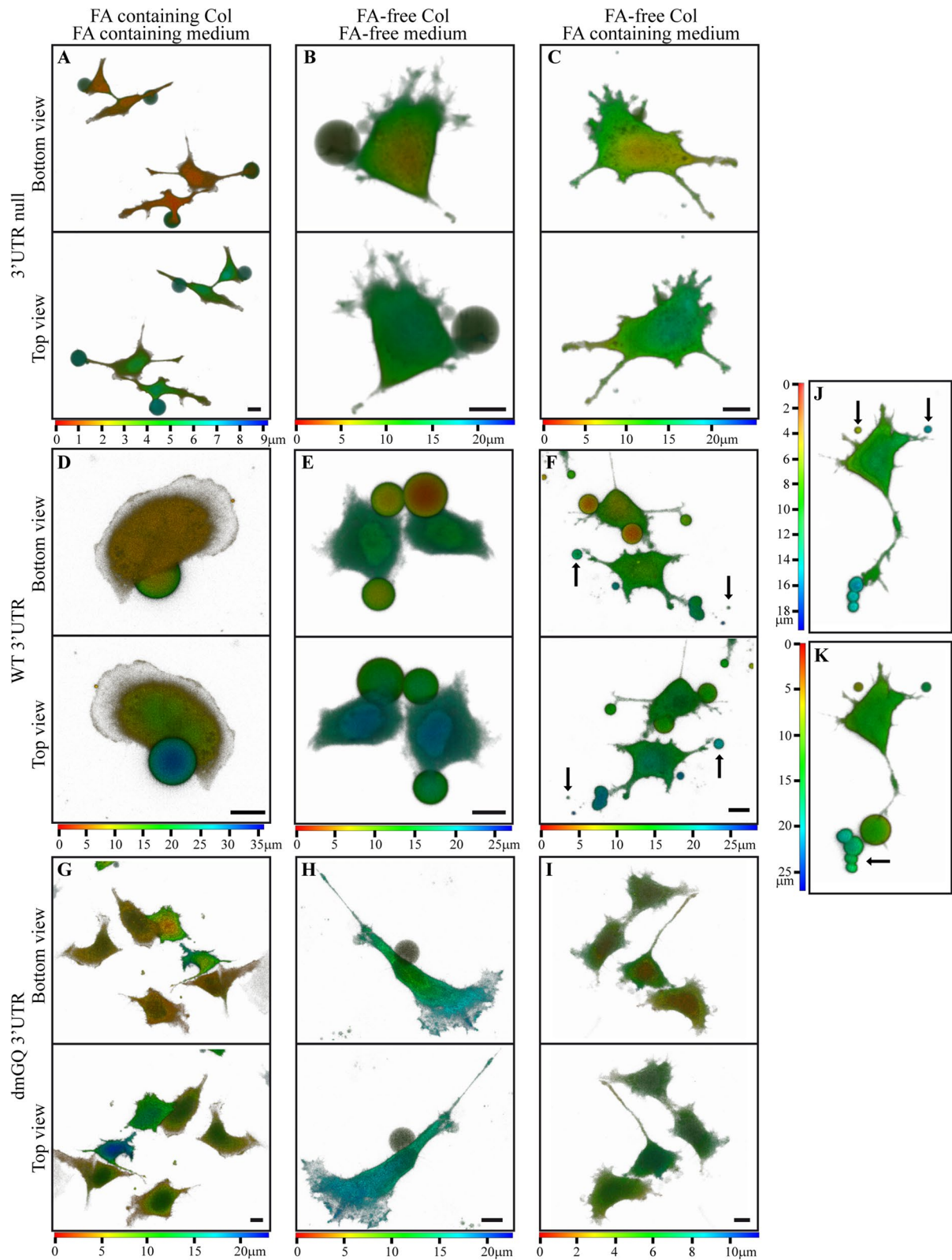
Fig. 8. (See legend on previous page.)

Stark *et al. BMC Biology*   (2023) 21:13

Page 15 of 23

the leading edge (pseudopods and blebs) was shown to have a higher cell mass density [148]. We therefor determined the fluorescence intensity of the cell body and the protruding blebs of the Col-invading cells as an indication of the cell mass (Table 2). Cells transfected with cFPGS expression vectors harboring either no-3′UTR or mutated 3′UTR exhibited lower fluorescence in the blebs compared to the cell body, with 3′UTR-dmGQ displaying a 4-fold lower bleb fluorescence. In contrast, cells harboring the WT-3′UTR exhibited up to 4-fold higher bleb fluorescence when compared to the cell body, corroborating the requirement of the FPGS 3′UTR for the development of invasive leading blebs.

Conclusions

Our novel findings reveal that the GQ motifs in the 3′UTR of FPGS regulate its transcript and protein localization at cell protrusions in response to a folate cue, thereby inducing cancer cell invasion. Previous studies by the group of S. Mili have shown that cancer cell invasion requires RNA localization at cell protrusions and the invasive front [56, 102, 154], hence suggesting RNA localization as a target for interference with cancer cell invasion. Along this vein, the FPGS 3′UTR GQs emerge in our present study as an attractive druggable target for the design of novel therapeutics. While inhibiting FPGS activity may be harmful to healthy tissues, impairing the cell protrusion localization of its mRNA by ASOs, targeted to the GQ motifs may inhibit invasion and metastasis. In recent years, DNA and RNA GQs have gained much interest as targets for antiviral [155, 156] and anticancer therapy [157, 158]; studies include, among others, inhibition of the translation of COVID-19 nucleocapsid phosphoprotein [159], inhibition of the translation of vascular endothelial growth factor [160], and suppression of c-myc transcription [161]. Thus, disruption of the subcellular localization of well-defined mRNAs may emerge as a novel targeted anticancer treatment strategy which may be enhanced when combined with chemotherapeutic as well as immunotherapeutic agents.

Methods
Chemicals and materials
RPMI-1640 medium (#21875034) and fetal bovine serum (#10270106) were from Gibco, Life Technologies, Grand Isle, NY. Glutamine, penicillin G, and streptomycin sulfate were from Biological Industries, Beit-Haemek, Israel. FA-free medium (#R1145), dialyzed fetal bovine serum (#F0392), and VBT (# V1377) were from Sigma-Aldrich, St. Louis, MO, USA. NCZ (#sc-3518), LAN B (#sc-203318), Y27632 (#sc-281642), and CyMl (#sc-500804) were from Santa Cruz Biotechnology, Dallas, TX, USA. Blebb (#13013) was from Cayman Chemical, Ann Arbor, MI, USA. FA (#J62937) was from Alfa Aesar, Tewksbury, MA, USA.

Tissue culture
Human cervical carcinoma HeLa cells (American Tissue Culture Collection, Manassas, VA) were maintained in RPMI-1640 medium supplemented with 10% FBS, 2 mM glutamine, 100 units/ml penicillin G, and 100 μg/ml streptomycin sulfate in a humidified atmosphere of 5% CO_2 at 37 °C. For folate deprivation, cells were grown in FA-free medium supplemented with 10% dialyzed FBS, 2 mM glutamine, 100 units/ml penicillin G, and 100 μg/ml streptomycin sulfate for 14 days.

Online prediction tools and databases
The 3′UTR sequence of FPGS was analyzed for possible regulatory elements using the following online prediction tools: (1) The microRNA database *miRBase* was used to search for microRNA binding sites; URL: http://www.

Table 2 Fluorescence intensity ratios between the protruding blebs and cell body of cells in 3D Col gel

Growth condition	FPGS 3′UTR	Fluorescence intensity ratio[a] bleb/cell body	*p* value vs. WT 3′UTR
FA-containing Col and medium	Null	0.75 ± 0.22	4.60E−12
	WT	3.91 ± 0.58	
	dmGQ	N.A.	
FA-free Col and medium	Null	0.58 ± 0.09	4.60E−08
	WT	4.03 ± 0.18	
	dmGQ	0.25 ± 0.08	2.50E−08
FA-free Col and FA-containing medium	Null	0.29 ± 0.08	2.20E−07
	WT	3.25 ± 0.58	
	dmGQ	N.A.	

N.A. not applicable since no blebs were visual

[a] The fluorescence intensity ratios presented are the mean values obtained from analysis of ~10 cells ± S.D.

program was used to predict and score RNA G-quadruplex elements; URL: https://bioinformatics.ramapo.edu/QGRS/index.php [163].

Expression vectors

Primers used in this section are detailed in Table 3 (Sigma-Aldrich). Restriction enzymes were from New England Biolabs (Ipswich, MA, USA). Vectors and inserts were purified using the Wizard PCR & Gel cleanup kit (#A9281, Promega, Madison, WI, USA). Ligations were performed using the DNA Ligation kit 2.1 (# 6022, TaKaRa Bio, Shiga, Japan). All plasmids were sequenced by an ABI 3730xl DNA analyzer (Applied Biosystems, Waltham, MA, USA).

The pRK5/FLAG-cFPGS expression vector (F-cFPGS), harboring the ORF of cFPGS with an N-terminal FLAG-tag, was previously described [26]. The pRK5/FLAG-cFPGS-3′UTR-MS2V6 vector (F-MS2), harboring the ORF of cFPGS with its 3′UTR and the MBSV6-loop system [59, 165] was generated as follows:

- Cloning of the 3′UTR sequence of FPGS was performed by 3′ rapid amplification of cDNA ends (3′-RACE) as follows: Following the isolation of total RNA from HeLa cells, using the TRI Reagent RNA Isolation Reagent (#T9424, Sigma-Aldrich), we performed reverse transcription with the High-Capacity cDNA Reverse Transcription Kit (#AB-4368814,

Thermo Fisher Scientific, Waltham, MA, USA) primed by a polyT adapter primer with a customized extension instead of random primers. A first-round PCR was performed using HY TAQ READT MIX (# EZ-3007, hylabs, Rehovot, Israel) with a specific target forward primer (FPGS EX11-up) and an adapter primer. A second PCR was performed using the product from the first round as template, the adapter primer, and a second target primer (FPGS Ex15-up) [164], located downstream of the first. The final PCR products were resolved on a 1% agarose gel, purified, and cloned using the pGEM-T-easy ligation kit (# A1360, Promega).

- The 3′UTR sequence was subcloned into the F-cFPGS expression vector as follows: The UTR sequence was PCR-amplified from the pGEM vector using primers NheI-UTR & UTR-HindIII. For cloning purposes, we introduced a nucleotide change c.T2514C (NM_004957.6) introducing a NheI restriction site in the F-cFPGS vector (F-cFPGS-V525A), using the QuickChange II site-directed mutagenesis (SDM) kit (#200523, Agilent technologies, Santa Clara, CA, USA) and the NheI-sdm primers. Following a NheI-HindIII digestion of the vector and 3′UTR-insert and their ligation, an F-cFPGS-V525A-3′UTR plasmid was generated. We corrected the nucleotide change by SDM (NheI-fix primers) to generate the vector pRK5/FLAG-cFPGS-3′UTR.

Table 3 Primers used in the current study

Application	Name	Sequence 5′-3′
3′-RACE	polyT adapter	GACGCGTGTGGACAGTCGATTTTTTTTTTTTTTTTTTTT
	FPGS EX11-up[a]	CAAAGGCATCCAGGCCAGG
	adapter	GACGCGTGTGGACAGTCGA
	FPGS Ex15-up	TCAGCCAAGGCCGAGACC
Cloning	NheI-UTR	TAA<u>GCTAGC</u>CACTGGCAGCCTGCACC
	UTR-HindII	AAA<u>AAGCTT</u>GACGCGTGTGGACAGTCG
	MS2-Fw	ACCATGATTACGCCAAGCTTG
	MS2-Rv	GTGAATTCGAGCTCGGTACCTC
	overhang-BFP	CAAACAACAAGATGTGGAAGGCGGTAG
	BFP-XhoI	CAAA<u>CTCGAG</u>AATTAAGCTTGTGCCCC
SDM[b]	NheI-sdm	GCCATCCATGT<u>GCTAG**C**</u>CACTGGCAGCCTGCACCTG
	NheI-fix	GCCATCCATGTGCTAG***T***CACTGGCAGCCTGCACCTG
	EcoRV-sdm	GGTGCCTTTTGTTTTTGG<u>***A***T***A***TC</u>CTGGTTCTGTCTAGACTGGCC
	GQ116-sdm	GATCTAGACTGGCCTAGG***TT***CCA***TT***GCTTTG***T***GATG***T***GAGGCCGGGAGAGGATGTC
	GQ377-sdm	CCTCCCAGTGCCTTCTG***T***GAAG***T***GAGAG***T***GCCTCTGCCTG***T***GACACTGCGGGACAGAG

[a] Ref [164]

[b] Only the sense sequence is given. SDM was performed with two complementary primers

Underlined sequences denote restriction sites

Nucleotides mutated by SDM are shown in bold and are italicized

- The subcloning of the 24xMS2V6 loops system was performed by PCR-amplifying the ~1.7 Kb MS2 sequence from the pET259-pUC57 24xMS2V6 plasmid (Addgene plasmid #104391) [59], using Q5 high-fidelity polymerase (#M0491, New England Biolabs) and the primers MS2-Fw & MS2-Rv, followed by digestion with SmaI & XbaI. An EcoRV restriction site was generated in the 3′UTR sequence of pRK5/FLAG-cFPGS-3′UTR by SDM with the EcoRV-sdm primers, followed by digestion with EcoRV & XbaI. Ligation yielded the vector F-MS2.

The F-MS2-mGQ116 and F-MS2-mGQ377 vectors, harboring mutated GQ sequences at the 3′UTR, were generated by SDM using primers GQ116-sdm and GQ377-sdm, respectively. Consecutive SDM reactions were used to generate the double mutant F-MS2-dmGQ. Mutating the GQ sequences did not affect the predicted miRNA-binding sites.

The pUbC-nls-ha-stdMCP-stdGFP (MCP-GFP) expression vector, harboring a synonymized tandem dimer MCP fused to synonymized tandem dimer GFP, was a gift from Prof. Robert Singer (Addgene plasmid # 98916) [166].

pcDNA3.1/ZNT1-Ruby was previously described [167]. pTurboRFP-C (#FP231) and pTurboGFP-N (#FP512) were from Evrogen (Moscow, Russia). To generate a pTurboBFP-C construct, BFP was PCR-amplified from mTagBFP2-TOMM20-N-10 (Addgene plasmid #55328) [168] using the Q5 high-fidelity polymerase and the primers hang-BFP & BFP-XhoI. The pTurboRFP-C vector and BFP insert were digested by AgeI and XhoI, and then ligated.

Transfections

All transfections were carried out using linear polyethylenimine (PEI, MW 25,000) transfection reagent (#23966, Polysciences, Warrington, PA, USA). Cells were seeded in 24-well plates (4×10^4 cells/well) 24 h prior to transfection. Transfections were performed using 1 µg DNA at a PEI-DNA ratio of 3:1. F-MS2 and MCP-GFP plasmids were co-transfected at a ratio of 2:1.

Immunofluorescence (IF) and live imaging microscopy

Cells grown in complete growth medium or at day 12 of FA deprivation were transfected with the indicated expression vectors. After 16 h, the growth medium was replaced and cells were allowed to recuperate for 2 h, following which cells were trypsinized, and seeded in Eppendorf's Cell Imaging 24-well plates (#EP0030741021, Hamburg, Germany). For FBS-deprivation, the growth medium was replaced with FBS-free medium for a 16-h incubation period. The next day (i.e., day 14 of FA

deprivation), cells were either fixed (as detailed below) or imaged after/during FBS or FA repletion using a confocal Zeiss LSM 710 inverted microscope (×63 magnification, Oberkochen, Germany) during incubation at 37°C in an atmosphere of 5% CO_2.

For IF microscopy, cells were washed with PBS and fixed for 15 min with a freshly prepared 4% formaldehyde solution. This was preceded by 1 h of pre-incubation with 0.1% DMSO (vehicle) or the following inhibitors: 40 µM VBT, 10 µM NCZ, 250 nM LAN B, 30 µM CyMl, 20 µM Y27632 or 15 µM Blebb, and 15-min co-incubation with 2 µM FA. Following fixation, cells were washed twice with PBS for 5 min, permeabilized with 0.1% Triton X-100 in PBS for 10 min followed by two washes with PBS. Cells were blocked for 1 h at room temperature (RT) with TBS buffer (10 mM Tris, 150 mM NaCl, pH 7.4) containing 20% skimmed milk and then incubated with primary antibodies for 1 h at RT: 1:330 mouse anti-FLAG M2 (#F1804, Sigma-Aldrich), 1:500 rabbit anti-α-tubulin (#ab4074, Abcam, Cambridge, UK), and 1:200 rabbit anti-calnexin (#ADI-SPA-860, Enzo Life Sciences, Farmingdale, NY, USA). Following three 5-min washes with PBS, cells were co-incubated with fluorescent secondary antibodies along with DyLight 650 Phalloidin (#12956, Cell Signaling Technology, Danvers, MA, USA), for 1 h at RT in the dark: 1:400 goat anti-mouse DyLight 405 #115-475-062, 1:400 donkey anti-mouse Cy3 #715-165-150, 1:400 donkey anti-rabbit Alexa Fluor 488 #711-545-152, or 1:400 donkey anti-rabbit DyLight 405 #711-475-152 (Jackson ImmunoResearch laboratories, West Grove, PA, USA). Cells were then washed three times with PBS for 5 min and once with DDW, topped with Fluoromount-G (#00-4958-02, Invitrogen, Carlsbad, CA, USA), and covered with 13-mm glass coverslips. Fluorescence was recorded using a confocal Zeiss LSM 710 microscope (×63 magnification), with excitation wavelengths of 405, 488, 543, and 630 nm. Focus stacking was performed with 1.5-µM intervals from the lowest plane in an upwards direction. Confocal microscopy images and movies were processed using the ZEN 3.0 SR black edition software (Carl Zeiss Vision GmbH, Oberkochen, Germany).

GQ conservation analysis

For analysis of GQ conservation, we obtained the 3′UTR sequences of FPGS from different species from the Entrez RefSeq database. For each sequence, we used the command line version of the QGRS mapper (https://bioinformatics.ramapo.edu/QGRS/index.php) with default parameters to find the highest scoring GQ in the 3′UTR sequences as well as 100 randomly shuffled sequences of each 3′UTR. The two top-scoring GQs in the actual sequence were compared with those of the randomized sequences, computing an empirical *P* value for both the

Stark *et al. BMC Biology*   (2023) 21:13

Page 18 of 23

top-scoring G quadruplex, as well as for the sum of the scores of the two top-scoring GQs. If no GQ was found by QGRS mapper, a score of zero was assigned. Empirical *P* values were computed by comparing the score of the actual 3′UTR sequence with the randomized ones. Box plots show the median, 1st and 3rd quartiles, and whiskers extend to the further points in the 1.5 times the interquartile range.

cFPGS mRNA localization analyses

To determine the percentage of cells with localized cFPGS mRNA, only cells with cytoplasmic MCP were considered; cells exhibiting only nuclear MCP were dismissed. Cells were scored as protrusion localized if the MCP signal was significantly higher in cell protrusion (one or more) than in the cell body.

GQ targeting with antisense oligonucleotides

HeLa cells at day 13 of FA-deprivation were transfected with F-MS2 and MCP-GFP along with one of the following ASOs at a DNA ratio of 2:1:1, respectively: a non-targeted control ASO-Ctr which served as a negative control, 5′-ATTCCGGAATTGACTGACTGACTGA. ASO-GQ116, 5′-CTCTCCCGGCCTCCCATCCCAAAG C. ASO-GQ377, 5′-GTCCCGCAGTGTCCCAGGCAG AGGC (Integrated DNA Technologies, Coralville, IA, USA). Cells were also transfected with a combination of ASO-GQ116 and ASO-GQ377 or with F-MS2 and MCP-GFP alone, to verify that the control oligo had no impact on RNA localization. Six h after transfections, the growth medium was replaced with fresh FA-free medium. A 15-min FA pulse was given to the cells 24 h after transfection, following which they were fixed with formaldehyde as described above. Cells were then scanned using a confocal microscope and manually counted for cFPGS mRNA localization analysis.

Inverted invasion assay

Inverted invasion assays were conducted according to the published protocol by McArdle et. al. [131]. Specifically, on day 10 of FA deprivation, cells were seeded in 24-well plates. The next day cells were co-transfected with either of the following expression vectors: F-cFPGS & pTurbo-BFP, F-MS2 & pTurbo-GFP, or F-MS2-dmGQ & pTurbo-RFP. On day 12, the growth medium containing the transfection reagent was replaced and the cells were allowed to recover for 2 h before they were trypsinized, mixed together, and seeded in three 35-mm glass-bottom plates (#200350, SPL Life Sciences, Gyeonggi-do, Korea). After 4 h, when the cells attached to the plate, the growth medium was removed and cells were overlaid with 150 μl Col hydrogel as follows: Using micropipette tips stored at −20ºC, we combined on ice RatCol rat tail Type I collagen solution (#5153, Advanced BioMatrix, San Diego, CA, USA) at a final concentration of 2.4 mg/ml, one 10th volume of FA-free 10xRPMI-1640 medium, 30 mM $NaHCO_3$ and FBS-containing RPMI-1640 medium either containing (one plate) or lacking FA (two plates); see Additional file 2: Figure S5 for the assay design. After 30 min of incubation at 37 °C, when the hydrogels solidified, a thin layer of grease was applied on the rim of each gel to prevent its detachment during the assay. Gels were immersed in growth medium either containing or lacking FA and the plates were incubated for 40 h in a humidified atmosphere of 5% CO_2 at 37°C.

The first attempts included a formaldehyde fixation step; however, even 1 h long fixation did not affect the gel-invading cells, as was seen by the unsuccessful actin staining with phalloidin. Hence, we abandoned fixation and visualized the cells by live fluorescence imaging using an LSM 710 confocal microscope.

Content density

Cells from the inverted invasion assays were analyzed for content density represented by the fluorescence of the exogenous fluorescent protein they express, i.e., BFP, GFP, and RFP. For the calculation of fluorescence intensity, the cell body was defined as the perinuclear region with the highest fluorescence. If multiple blebs were present per cell, the bleb with the highest fluorescence was selected for the analysis. The regions of interest, i.e., cell body and blebs, were marked manually and measured throughout the recorded Z-stacks using the ImageJ software (version 1.52i, Wayne Rasband National Institute of Health, Washington, DC, USA). The fluorescence value is the mean fluorescence recorded in each 3D area.

Statistical analyses

For the quantification of changes in cell percentage with localized cFPGS mRNA, a two-tailed paired Student *t*-test was performed. For the number of protrusions per cell and cell content density, a two-tailed two-sample equal variance Student t-test was performed. *p* values ≤ 0.05 were considered statistically significant and are given in the Figure legends and Table 2.

Abbreviations

GTPases	Guanosine triphosphatases
RhoA	Ras homolog family member A
Rac1	Ras-related C3 botulinum toxin substrate 1
CDC42	Cell division control protein 42 homolog
SAM/AdoMet	S-Adenosylmethionine
5-CH3-THF	5-Methyl-tetrahydrofolate
FPGS	Folylpolyglutamate synthetase
cFPGS	Cytosolic FPGS
GQ	G-quadruplex
FA	Folic acid
CFL1	Cofilin 1

VCL	Vinculin
FSCN1	Fascin
CTTN	Cortactin
IQGAP1	IQ motif containing GTPase-activating protein 1
TLN1	Talin-1
IF	Immunofluorescence
ARP2/3	Actin-related protein 2/3 complex
RAB13	Ras-related protein Rab-13
STAT3	Signal transducer and activator of transcription 3
F-cFPGS	pRK5/FLAG-cFPGS
F-MS2	pRK5/FLAG-cFPGS-3'UTR-MS2V6
MCP	MS2-coat protein
RBP	RNA binding protein
GQBP	GQ-binding protein
FMRP/FMR1	Fragile X mental retardation protein 1
DDX3	DEAD box protein 3, X isoform
FUS	Fused in sarcoma
CAMK2A	Calcium/calmodulin-dependent protein kinase type II subunit alpha
FLNA	Filamin A
FLNB	Filamin B
ACTR2	Actin-related protein 2
ARPC4	Actin-related protein 2/3 complex subunit 4
CAPZB	F-Actin-capping protein subunit beta
FBS	Fetal bovine serum
F-actin	Filamentous actin
F-MS2-dmGQ	Double GQ mutant F-MS2
ASO	Antisense oligonucleotide
APC	Adenomatous polyposis coli
ZBP1	Zipcode binding protein 1
VBT	Vinblastine
α-Tub	α-Tubulin
NCZ	Nocodazole
LAN B	Latrunculin B
CANX	Calnexin
pCFL1	Phosphorylated CFL1
ROCK	Rho-associated protein kinase
CyMl	Cysmethynil
ICMT	Protein-S-isoprenylcysteine O-methyltransferase
Blebb	Blebbistatin
Col	Collagen

Supplementary Information

The online version contains supplementary material available at https://doi.org/10.1186/s12915-023-01525-1.

Additional file 1: Table S1. G-quadruplex sequences found by QGRS Mapper in the 3'UTR of FPGS orthologs.

Additional file 2: Figures S1-S6. Figure S1. G scores for GQ motifs in the 3'UTR of FPGS orthologues. **Figure S2.** IF microscopy of VBT treated cells. **Figure S3.** Live imaging of FPGS RNA localization in VBT treated cells. **Figure S4.** IF microscopy suggesting the localization of FPGS translation. **Figure S5.** Design of cell migration assay under collagen-confined conditions. **Figure S6.** Cell morphology within collagen gel. Legends to movies S1-S9.

Additional file 3: Movie S1. F-cFPGS & BFP harboring cells in FA-containing collagen.

Additional file 4: Movie S2. An F-cFPGS & BFP harboring cell in FA-free collagen.

Additional file 5: Movie S3. An F-cFPGS & BFP harboring cell in FA-free collagen immersed in FA-containing medium.

Additional file 6: Movie S4. An F-MS2 & GFP harboring cell in FA-containing collagen.

Additional file 7: Movie S5. F-MS2 & GFP harboring cells in FA-free collagen.

Additional file 8: Movie S6. F-MS2 & GFP harboring cells in FA-free collagen immersed in FA-containing medium.

Additional file 9: Movie S7. F-MS2-dmGQ & RFP harboring cells in FA-containing collagen.

Additional file 10: Movie S8. An F-MS2-dmGQ & RFP harboring cell in FA-free collagen.

Additional file 11: Movie S9. F-MS2-dmGQ & RFP harboring cells in FA-free collagen immersed in FA-containing medium.

Availability of data and materials
All data generated or analyzed during this study are included in this published article (and its supplementary information files).

Declarations

Ethics approval and consent to participate
Not applicable.

Consent for publication
Not applicable.

Competing interests
The authors declare that they have no competing interests.

References

1. Li X, Miao Y, Pal DS, Devreotes PN. Excitable networks controlling cell migration during development and disease. Semin Cell Dev Biol. 2020;100:133–42.
2. Worbs T, Hammerschmidt SI, Förster R. Dendritic cell migration in health and disease. Nat Rev Immunol. 2017;17:30–48.
3. Guak H, Krawczyk CM. Implications of cellular metabolism for immune cell migration. Immunology. 2020;161:200–8.
4. Trepat X, Chen Z, Jacobson K. Cell migration. Compr Physiol. 2012;2:2369–92.
5. Lawson CD, Ridley AJ. Rho GTPase signaling complexes in cell migration and invasion. J Cell Biol. 2018;217:447–57.
6. Warner H, Wilson BJ, Caswell PT. Control of adhesion and protrusion in cell migration by rho GTPases. Curr Opin Cell Biol. 2019;56:64–70.
7. Guan X, Guan X, Dong C, Jiao Z. Rho GTPases and related signaling complexes in cell migration and invasion. Exp Cell Res. 2020;388:111824.
8. Cushman I, Casey PJ. RHO methylation matters: a role for isoprenylcysteine carboxylmethyltransferase in cell migration and adhesion. Cell Adhes Migr. 2011;5:11–5.
9. Cushman I, Casey PJ. Role of isoprenylcysteine carboxylmethyltransferase-catalyzed methylation in rho function and migration. J Biol Chem. 2009;284:27964–73.
10. Oleinik NV, Helke KL, Kistner-Griffin E, Krupenko NI, Krupenko SA. Rho GTPases RhoA and Rac1 mediate effects of dietary folate on metastatic potential of A549 cancer cells through the control of cofilin phosphorylation. J Biol Chem. 2014;289:26383–94.

Stark *et al. BMC Biology*   (2023) 21:13

Page 20 of 23

11. Backlund PS. Post-translational processing of RhoA. Carboxyl methylation of the carboxyl-terminal prenylcysteine increases the half-life of Rhoa. J Biol Chem. 1997;272:33175–80.

12. Cansado J. To finish things well: cysteine methylation ensures selective GTPase membrane localization and signalling. Curr Genet. 2018;64:341–4.

13. Sun Q, Huang M, Wei Y. Diversity of the reaction mechanisms of SAM-dependent enzymes. Acta Pharm Sin B. 2021;11:632–50.

14. Fox JT, Stover PJ. Folate-mediated one-carbon metabolism. Vitam Horm. 2008;79:1–44.

15. Froese DS, Fowler B, Baumgartner MR. Vitamin B 12 , folate, and the methionine remethylation cycle-biochemistry, pathways, and regulation. J Inherit Metab Dis. 2019;42:673–85.

16. Scott JM. Folate and vitamin B12. Proc Nutr Soc. 1999;58:441–8.

17. Rosenberg IH. A history of the isolation and identification of folic acid (folate). Ann Nutr Metab. 2012;61:231–5.

18. Zhao R, Diop-Bove N, Visentin M, Goldman ID. Mechanisms of membrane transport of folates into cells and across epithelia. Annu Rev Nutr. 2011;31:177–201.

19. Raz S, Stark M, Assaraf YG. Folylpoly-γ-glutamate synthetase: a key determinant of folate homeostasis and antifolate resistance in cancer. Drug Resist Updat. 2016;28:43–64.

20. McGuire JJ, Hsieh P, Coward JK, Bertino JR. Enzymatic synthesis of folylpolyglutamates. Characterization of the reaction and its products. J Biol Chem. 1980;255:5776–88.

21. Kamen BA, Capdevila A. Receptor-mediated folate accumulation is regulated by the cellular folate content. Proc Natl Acad Sci U S A. 1986;83:5983–7.

22. Hoppner K, Lampi B. Folate levels in human liver from autopsies in Canada. Am J Clin Nutr. 1980;33:862–4.

23. Garrow TA, Admon A, Shane B. Expression cloning of a human cDNA encoding folylpoly(gamma-glutamate) synthetase and determination of its primary structure. Proc Natl Acad Sci U S A. 1992;89:9151–5.

24. Freemantle SJ, Taylor SM, Krystal G, Moran RG. Upstream organization of and multiple transcripts from the human folylpoly-gamma-glutamate synthetase gene. J Biol Chem. 1995;270:9579–84.

25. Lawrence SA, Titus SA, Ferguson J, Heineman AL, Taylor SM, Moran RG. Mammalian mitochondrial and cytosolic folylpolyglutamate synthetase maintain the subcellular compartmentalization of folates. J Biol Chem. 2014;289:29386–96.

26. Stark M, Raz S, Assaraf YG. Folylpoly-ɣ-glutamate synthetase association to the cytoskeleton: implications to folate metabolon compartmentalization. J Proteome. 2021;239:104169.

27. Banco MT, Ferré-D'Amaré AR. The emerging structural complexity of G-quadruplex RNAs. RNA. 2021;27:390–402.

28. Lipps HJ, Rhodes D. G-quadruplex structures: in vivo evidence and function. Trends Cell Biol. 2009;19:414–22.

29. Hänsel-Hertsch R, Di Antonio M, Balasubramanian S. DNA G-quadruplexes in the human genome: detection, functions and therapeutic potential. Nat Rev Mol Cell Biol. 2017;18:279–84.

30. Varshney D, Spiegel J, Zyner K, Tannahill D, Balasubramanian S. The regulation and functions of DNA and RNA G-quadruplexes. Nat Rev Mol Cell Biol. 2020;21:459–74.

31. Besnard E, Babled A, Lapasset L, Milhavet O, Parrinello H, Dantec C, et al. Unraveling cell type-specific and reprogrammable human replication origin signatures associated with G-quadruplex consensus motifs. Nat Struct Mol Biol. 2012;19:837–44.

32. Phan AT. Human telomeric G-quadruplex: structures of DNA and RNA sequences. FEBS J. 2010;277:1107–17.

33. Lee DSM, Ghanem LR, Barash Y. Integrative analysis reveals RNA G-quadruplexes in UTRs are selectively constrained and enriched for functional associations. Nat Commun. 2020;11:527.

34. Bedrat A, Lacroix L, Mergny JL. Re-evaluation of G-quadruplex propensity with G4Hunter. Nucleic Acids Res. 2016;44:1746–59.

35. Subramanian M, Rage F, Tabet R, Flatter E, Mandel JL, Moine H. G-quadruplex RNA structure as a signal for neurite mRNA targeting. EMBO Rep. 2011;12:697–704.

36. Darnell JC, Jensen KB, Jin P, Brown V, Warren ST, Darnell RB. Fragile X mental retardation protein targets G quartet mRNAs important for neuronal function. Cell. 2001;107:489–99.

37. Aune D, Deneo-Pellegrini H, Ronco AL, Boffetta P, Acosta G, Mendilaharsu M, et al. Dietary folate intake and the risk of 11 types of cancer: a case–control study in Uruguay. Ann Oncol. 2011;22:444–51.

38. Cantarella CD, Ragusa D, Giammanco M, Tosi S. Folate deficiency as predisposing factor for childhood leukaemia: a review of the literature. Genes Nutr. 2017;12:14.

39. Pieroth R, Paver S, Day S, Lammersfeld C. Folate and its impact on cancer risk. Curr Nutr Rep. 2018;7:70.

40. Kim YI. Role of folate in colon cancer development and progression. J Nutr. 2003;133(11 Suppl 1):3731S–3739S.

41. Lee TY, Chiang EP, Shih YT, Lane HY, Lin JT, Wu CY. Lower serum folate is associated with development and invasiveness of gastric cancer. World J Gastroenterol. 2014;20:11313–20.

42. Su YH, Huang WC, Huang TH, Huang YJ, Sue YK, Huynh TT, et al. Folate deficient tumor microenvironment promotes epithelial-to-mesenchymal transition and cancer stem-like phenotypes. Oncotarget. 2016;7:33246–56.

43. Kuo CS, Lin CY, Wu MY, Lu CL, Huang RF. Relationship between folate status and tumour progression in patients with hepatocellular carcinoma. Br J Nutr. 2008;100:596–602.

44. Jacquemet G, Hamidi H, Ivaska J. Filopodia in cell adhesion, 3D migration and cancer cell invasion. Curr Opin Cell Biol. 2015;36:23–31.

45. Augoff K, Hryniewicz-Jankowska A, Tabola R. Invadopodia: clearing the way for cancer cell invasion. Ann Transl Med. 2020;8:902.

46. Beaty BT, Condeelis J. Digging a little deeper: the stages of invadopodium formation and maturation. Eur J Cell Biol. 2014;93:438–44.

47. Willett M, Brocard M, Pollard HJ, Morley SJ. mRNA encoding WAVE-Arp2/3-associated proteins is co-localized with foci of active protein synthesis at the leading edge of MRC5 fibroblasts during cell migration. Biochem J. 2013;452:45–55.

48. Maizels Y, Oberman F, Miloslavski R, Ginzach N, Berman M, Yisraeli JK. Localization of cofilin mRNA to the leading edge of migrating cells promotes directed cell migration. J Cell Sci. 2015;128:1922–33.

49. Babic I, Sharma S, Black DL. A role for polypyrimidine tract binding protein in the establishment of focal adhesions. Mol Cell Biol. 2009;29:5564–77.

50. Mingle LA, Okuhama NN, Shi J, Singer RH, Condeelis J, Liu G. Localization of all seven messenger RNAs for the actin-polymerization nucleator Arp2/3 complex in the protrusions of fibroblasts. J Cell Sci. 2005;118(Pt 11):2425–33.

51. Oleynikov Y, Singer RH. Real-time visualization of ZBP1 association with beta-actin mRNA during transcription and localization. Curr Biol. 2003;13:199–207.

52. Tushev G, Glock C, Heumüller M, Biever A, Jovanovic M, Schuman EM. Alternative 3′UTRs modify the localization, regulatory potential, stability, and plasticity of mRNAs in neuronal compartments. Neuron. 2018;98:495–511.e6.

53. Mattioli CC, Rom A, Franke V, Imami K, Arrey G, Terne M, et al. Alternative 3′UTRs direct localization of functionally diverse protein isoforms in neuronal compartments. Nucleic Acids Res. 2019;47:2560–73.

54. Bauer KE, Segura I, Gaspar I, Scheuss V, Illig C, Ammer G, et al. Live cell imaging reveals 3′-UTR dependent mRNA sorting to synapses. Nat Commun. 2019;10:3178.

55. Kislauskis EH, Li Z, Singer RH, Taneja KL. Isoform-specific 3′-untranslated sequences sort alpha-cardiac and beta-cytoplasmic actin messenger RNAs to different cytoplasmic compartments. J Cell Biol. 1993;123:165–72.

56. Moissoglu K, Stueland M, Gasparski AN, Wang T, Jenkins LM, Hastings ML, et al. RNA localization and co-translational interactions control RAB13 GTPase function and cell migration. EMBO J. 2020;39:e104958.

57. Shen Z, Liu B, Wu B, Zhou H, Wang X, Cao J, et al. FMRP regulates STAT3 mRNA localization to cellular protrusions and local translation to promote hepatocellular carcinoma metastasis. Commun Biol. 2021;4:540.

58. Liu YH, Jin JL, Wang YZ, Tan Y, Zhou YY, Peng T, et al. Protrusion-localized STAT3 mRNA promotes metastasis of highly metastatic hepatocellular carcinoma cells in vitro. Acta Pharmacol Sin. 2016;37:805–13.

59. Tutucci E, Vera M, Biswas J, Garcia J, Parker R, Singer RH. An improved MS2 system for accurate reporting of the mRNA life cycle. Nat Methods. 2018;15:81–9.

Stark *et al. BMC Biology*   (2023) 21:13

Page 21 of 23

60. Jia Z, Barbier L, Stuart H, Amraei M, Pelech S, Dennis JW, et al. Tumor cell pseudopodial protrusions. Localized signaling domains coordinating cytoskeleton remodeling, cell adhesion, glycolysis, RNA translocation, and protein translation. J Biol Chem. 2005;280:30564–73.

61. Goering R, Hudish LI, Guzman BB, Raj N, Bassell GJ, Russ HA, et al. FMRP promotes RNA localization to neuronal projections through interactions between its RGG domain and G-quadruplex RNA sequences. Elife. 2020;9:1–31.

62. Zhang Y, Gaetano CM, Williams KR, Bassell GJ, Mihailescu MR. FMRP interacts with G-quadruplex structures in the 3'-UTR of its dendritic target Shank1 mRNA. RNA Biol. 2014;11:1364–74.

63. Herdy B, Mayer C, Varshney D, Marsico G, Murat P, Taylor C, et al. Analysis of NRAS RNA G-quadruplex binding proteins reveals DDX3X as a novel interactor of cellular G-quadruplex containing transcripts. Nucleic Acids Res. 2018;46:11592–604.

64. Imperatore JA, McAninch DS, Valdez-Sinon AN, Bassell GJ, Mihailescu MR. FUS recognizes G quadruplex structures within neuronal mRNAs. Front Mol Biosci. 2020;7:6.

65. Kanai Y, Dohmae N, Hirokawa N. Kinesin transports RNA: isolation and characterization of an RNA-transporting granule. Neuron. 2004;43:513–25.

66. Yasuda K, Zhang H, Loiselle D, Haystead T, Macara IG, Mili S. The RNA-binding protein Fus directs translation of localized mRNAs in APC-RNP granules. J Cell Biol. 2013;203:737–46.

67. Jakobsen KR, Sørensen E, Brøndum KK, Daugaard TF, Thomsen R, Nielsen AL. Direct RNA sequencing mediated identification of mRNA localized in protrusions of human MDA-MB-231 metastatic breast cancer cells. J Mol Signal. 2013;8:9.

68. Mardakheh FK, Paul A, Kümper S, Sadok A, Paterson H, Mccarthy A, et al. Global analysis of mRNA, translation, and protein localization: local translation is a key regulator of cell protrusions. Dev Cell. 2015;35:344–57.

69. Chouaib R, Safieddine A, Pichon X, Imbert A, Kwon OS, Samacoits A, et al. A dual protein-mRNA localization screen reveals compartmentalized translation and widespread co-translational RNA targeting. Dev Cell. 2020;54:773–791.e5.

70. Shankar J, Messenberg A, Chan J, Underhill TM, Foster LJ, Nabi IR. Pseudopodial actin dynamics control epithelial-mesenchymal transition in metastatic cancer cells. Cancer Res. 2010;70:3780–90.

71. Liao G, Simone B, Liu G. Mis-localization of Arp2 mRNA impairs persistence of directional cell migration. Exp Cell Res. 2011;317:812–22.

72. Mayford M, Baranes D, Podsypanina K, Kandel ER. The 3'-untranslated region of CaMKII alpha is a cis-acting signal for the localization and translation of mRNA in dendrites. Proc Natl Acad Sci U S A. 1996;93:13250–5.

73. Mikl M, Vendra G, Kiebler MA. Independent localization of MAP2, CaMKIIα and β-actin RNAs in low copy numbers. EMBO Rep. 2011;12:1077–84.

74. Qin M, Chen Z, Luo Q, Wen Y, Zhang N, Jiang H, et al. Two-quartet G-quadruplexes formed by DNA sequences containing four contiguous GG runs. J Phys Chem B. 2015;119:3706–13.

75. Islam B, Stadlbauer P, Vorlíčková M, Mergny JL, Otyepka M, Šponer J. Stability of two-quartet G-quadruplexes and their dimers in atomistic simulations. J Chem Theory Comput. 2020;16:3447–63.

76. Ceschi S, Largy E, Gabelica V, Sissi C. A two-quartet G-quadruplex topology of human KIT2 is conformationally selected by a perylene derivative. Biochimie. 2020;179:77–84.

77. Ishiguro A, Kimura N, Watanabe Y, Watanabe S, Ishihama A. TDP-43 binds and transports G-quadruplex-containing mRNAs into neurites for local translation. Genes Cells. 2016;21:466–81.

78. Feuge J, Scharkowski F, Michaelsen-Preusse K, Korte M. FMRP modulates activity-dependent spine plasticity by binding cofilin1 mRNA and regulating localization and local translation. Cereb Cortex. 2019;29:5204–16.

79. Kao DI, Aldridge GM, Weiler IJ, Greenough WT. Altered mRNA transport, docking, and protein translation in neurons lacking fragile X mental retardation protein. Proc Natl Acad Sci U S A. 2010;107:15601–6.

80. Brown V, Jin P, Ceman S, Darnell JC, O'Donnell WT, Tenenbaum SA, et al. Microarray identification of FMRP-associated brain mRNAs and altered mRNA translational profiles in fragile X syndrome. Cell. 2001;107:477–87.

81. Razinia Z, Mäkelä T, Ylänne J, Calderwood DA. Filamins in mechanosensing and signaling. Annu Rev Biophys. 2012;41:227–46.

82. Casingal CR, Kikkawa T, Inada H, Sasaki Y, Osumi N. Identification of FMRP target mRNAs in the developmental brain: FMRP might coordinate Ras/MAPK, Wnt/β-catenin, and mTOR signaling during corticogenesis. Mol Brain. 2020;13:167.

83. Qi T, Xu Y, Zhou T, Gu W. The evolution of G-quadruplex structure in mRNA untranslated region. Evol Bioinformatics Online. 2021;17:11769343211035140.

84. Lin YH, Bundschuh R. RNA structure generates natural cooperativity between single-stranded RNA binding proteins targeting 5' and 3'UTRs. Nucleic Acids Res. 2015;43:1160–9.

85. Masai H, Fukatsu R, Kakusho N, Kanoh Y, Moriyama K, Ma Y, et al. Rif1 promotes association of G-quadruplex (G4) by its specific G4 binding and oligomerization activities. Sci Rep. 2019;9:8618.

86. Kolesnikova S, Curtis EA. Structure and function of multimeric G-quadruplexes. Molecules. 2019;24:3074.

87. Frasson I, Pirota V, Richter SN, Doria F. Multimeric G-quadruplexes: a review on their biological roles and targeting. Int J Biol Macromol. 2022;204:89–102.

88. Loughlin FE, Lukavsky PJ, Kazeeva T, Reber S, Hock EM, Colombo M, et al. The solution structure of FUS bound to RNA reveals a bipartite mode of RNA recognition with both sequence and shape specificity. Mol Cell. 2019;73:490–504.e6.

89. Chao JA, Patskovsky Y, Patel V, Levy M, Almo SC, Singer RH. ZBP1 recognition of beta-actin zipcode induces RNA looping. Genes Dev. 2010;24:148–58.

90. Moissoglu K, Yasuda K, Wang T, Chrisafis G, Mili S. Translational regulation of protrusion-localized RNAs involves silencing and clustering after transport. Elife. 2019;8:e44752.

91. Pan M, Xu X, Chen Y, Jin T. Identification of a chemoattractant G-protein-coupled receptor for folic acid that controls both Chemotaxis and phagocytosis. Dev Cell. 2016;36:428–39.

92. Pan P, Hall EM, Bonner JT. Folic acid as second chemotactic substance in the cellular slime moulds. Nat New Biol. 1972;237:181–2.

93. Maeda Y, Mayanagi T, Amagai A. Folic acid is a potent chemoattractant of free-living amoebae in a new and amazing species of protist, Vahlkampfia sp. Zoolog Sci. 2009;26:179–86.

94. Aufderheide KJ, Janetopoulos C. Migration of dictyostelium discoideum to the chemoattractant folic acid. Methods Mol Biol. 2016;1407:25–39.

95. Petersen LF, Brockton NT, Bakkar A, Liu S, Wen J, Weljie AM, et al. Elevated physiological levels of folic acid can increase in vitro growth and invasiveness of prostate cancer cells. BJU Int. 2012;109:788–95.

96. Wang Z, Wang W, Zhao W, Wang Z, Yang J, Wang W, et al. Folate inhibits miR-27a-3p expression during cervical carcinoma progression and oncogenic activity in human cervical cancer cells. Biomed Pharmacother. 2020;122:109654.

97. Zhao H, Wong HY, Ji D, Lyu K, Kwok CK. Novel L-RNA aptamer controls APP gene expression in cells by targeting RNA G-quadruplex structure. ACS Appl Mater Interfaces. 2022;14:30582–94.

98. Bhattacharyya D, Nguyen K, Basu S. Rationally induced RNA:DNA G-Quadruplex structures elicit an anticancer effect by inhibiting endogenous eIF-4E expression. Biochemistry. 2014;53:5461–70.

99. Rouleau SG, Beaudoin JD, Bisaillon M, Perreault JP. Small antisense oligonucleotides against G-quadruplexes: specific mRNA translational switches. Nucleic Acids Res. 2015;43:595–606.

100. Lai A, Valdez-Sinon AN, Bassell GJ. Regulation of RNA granules by FMRP and implications for neurological diseases. Traffic. 2020;21:454–62.

101. Mili S, Moissoglu K, Macara IG. Genome-wide screen reveals APC-associated RNAs enriched in cell protrusions. Nature. 2008;453:115–9.

102. Wang T, Hamilla S, Cam M, Aranda-Espinoza H, Mili S. Extracellular matrix stiffness and cell contractility control RNA localization to promote cell migration. Nat Commun. 2017;8:896.

103. Pichon X, Moissoglu K, Coleno E, Wang T, Imbert A, Robert MC, et al. The kinesin KIF1C transports APC-dependent mRNAs to cell protrusions. RNA. 2021;27:1528–44.

104. Eom T, Antar LN, Singer RH, Bassell GJ. Localization of a beta-actin messenger ribonucleoprotein complex with zipcode-binding protein modulates the density of dendritic filopodia and filopodial synapses. J Neurosci. 2003;23:10433–44.

105. Ross AF, Oleynikov Y, Kislauskis EH, Taneja KL, Singer RH. Characterization of a beta-actin mRNA zipcode-binding protein. Mol Cell Biol. 1997;17:2158–65.

106. Vasilyev N, Polonskaia A, Darnell JC, Darnell RB, Patel DJ, Serganov A. Crystal structure reveals specific recognition of a G-quadruplex RNA by a β-turn in the RGG motif of FMRP. Proc Natl Acad Sci U S A. 2015;112:E5391–400.

107. Antar LN, Dictenberg JB, Plociniak M, Afroz R, Bassell GJ. Localization of FMRP-associated mRNA granules and requirement of microtubules for activity-dependent trafficking in hippocampal neurons. Genes Brain Behav. 2005;4:350–9.

108. Wang H, Dictenberg JB, Ku L, Li W, Bassell GJ, Feng Y. Dynamic association of the fragile X mental retardation protein as a messenger ribonucleoprotein between microtubules and polyribosomes. Mol Biol Cell. 2008;19:105–14.

109. Gigant B, Wang C, Ravelli RBG, Roussi F, Steinmetz MO, Curmi PA, et al. Structural basis for the regulation of tubulin by vinblastine. Nature. 2005;435:519–22.

110. Bensch KG, Malawista SE. Microtubular crystals in mammalian cells. J Cell Biol. 1969;40:95–107.

111. Manfredi JJ, Horwitz SB. Vinblastine paracrystals from cultured cells are calcium-stable. Exp Cell Res. 1984;150:205–12.

112. De Brabander MJ, Van de Veire RML, Aerts FEM, Borgers M, Janssan PAJ. The effects of methyl [5-(2-thienylcarbonyl)-1H-benzimidazol-2-yl] carbamate, (R 17934; NSC 238159), a new synthetic antitumoral drug interfering with microtubules, on mammalian cells cultured in vitro. Cancer Res. 1976;36:905–16.

113. Bernier LP, Bohlen CJ, York EM, Choi HB, Kamyabi A, Dissing-Olesen L, et al. Nanoscale surveillance of the brain by microglia via cAMP-regulated filopodia. Cell Rep. 2019;27:2895–2908.e4.

114. Horev MB, Zabary Y, Zarka R, Sorrentino S, Medalia O, Zaritsky A, et al. Differential dynamics of early stages of platelet adhesion and spreading on collagen IV and fibrinogen-coated surfaces [version 2; peer review: 3 approved]. F1000Research. 2021;9:1–27.

115. Nufer O, Guldbrandsen S, Degen M, Kappeler F, Paccaud JP, Tani K, et al. Role of cytoplasmic C-terminal amino acids of membrane proteins in ER export. J Cell Sci. 2002;115 Pt 3:619–28.

116. Crambert G, Li C, Swee LK, Geering K. FXYD7, mapping of functional sites involved in endoplasmic reticulum export, association with and regulation of Na, K-ATPase. J Biol Chem. 2004;279:30888–95.

117. Latham VM, Yu EHS, Tullio AN, Adelstein RS, Singer RH. A rho-dependent signaling pathway operating through myosin localizes beta-actin mRNA in fibroblasts. Curr Biol. 2001;11:1010–6.

118. Stuart HC, Jia Z, Messenberg A, Joshi B, Underhill TM, Moukhles H, et al. Localized rho GTPase activation regulates RNA dynamics and compartmentalization in tumor cell protrusions. J Biol Chem. 2008;283:34785–95.

119. Oleinik NV, Krupenko NI, Krupenko SA. ALDH1L1 inhibits cell motility via dephosphorylation of cofilin by PP1 and PP2A. Oncogene. 2010;29:6233–44.

120. Gungabissoon RA, Bamburg JR. Regulation of growth cone actin dynamics by ADF/cofilin. J Histochem Cytochem. 2003;51:411–20.

121. Sumi T, Matsumoto K, Takai Y, Nakamura T. Cofilin phosphorylation and actin cytoskeletal dynamics regulated by rho- and Cdc42-activated LIM-kinase 2. J Cell Biol. 1999;147:1519–32.

122. Cushman I, Cushman SM, Potter PM, Casey PJ. Control of RhoA methylation by carboxylesterase I. J Biol Chem. 2013;288:19177–83.

123. Abbasi IHR, Abbasi F, Wang L, Abd El Hack ME, Swelum AA, Hao R, et al. Folate promotes S-adenosyl methionine reactions and the microbial methylation cycle and boosts ruminants production and reproduction. AMB Express. 2018;8:65.

124. Baron RA, Peterson YK, Otto JC, Rudolph J, Casey PJ. Time-dependent inhibition of isoprenylcysteine carboxyl methyltransferase by indole-based small molecules. Biochemistry. 2007;46:554–60.

125. Winter-Vann AM, Baron RA, Wong W, Dela Cruz J, York JD, Gooden DM, et al. A small-molecule inhibitor of isoprenylcysteine carboxyl methyltransferase with antitumor activity in cancer cells. Proc Natl Acad Sci U S A. 2005;102:4336–41.

126. Rounds S, Lu Q, Harrington EO, Newton J, Casserly B. Pulmonary endothelial cell signaling and function. Trans Am Clin Climatol Assoc. 2008;119:155.

127. Pan P, Shen M, Yu H, Li Y, Li D, Hou T. Advances in the development of rho-associated protein kinase (ROCK) inhibitors. Drug Discov Today. 2013;18:1323–33.

128. Straight AF, Cheung A, Limouze J, Chen I, Westwood NJ, Sellers JR, et al. Dissecting temporal and spatial control of cytokinesis with a myosin II inhibitor. Science. 2003;299:1743–7.

129. Kovács M, Tóth J, Hetényi C, Málnási-Csizmadia A, Seller JR. Mechanism of blebbistatin inhibition of myosin II. J Biol Chem. 2004;279:35557–63.

130. McArdle TJ, Ogle BM, Noubissi FK. An in vitro inverted vertical invasion assay to avoid manipulation of rare or sensitive cell types. J Cancer. 2016;7:2333–40.

131. McArdle TJ, Ogle BM, Noubissi FK. Moving upwards: a simple and flexible in vitro three-dimensional invasion assay protocol. J Vis Exp. 2018;133:56568.

132. Corning. Matrigel Matrix Produc Data. https://www.corning.com/catalog/cls/documents/faqs/CLS-DL-CC-026.pdf. Accessed 2022

133. TREVIGEN. Cultrex ® Reduced Growth Factor Basement Membrane Extract, Type R1, PathClear ® Product Data. https://fnkprddata.blob.core.windows.net/domestic/data/datasheet/RSD/3433-001-R1.pdf. Accessed 2022.

134. Lessey EC, Guilluy C, Burridge K. From mechanical force to RhoA activation. Biochemistry. 2012;51:7420–32.

135. Liu YJ, Le Berre M, Lautenschlaeger F, Maiuri P, Callan-Jones A, Heuzé M, et al. Confinement and low adhesion induce fast amoeboid migration of slow mesenchymal cells. Cell. 2015;160:659–72.

136. Lang NR, Skodzek K, Hurst S, Mainka A, Steinwachs J, Schneider J, et al. Biphasic response of cell invasion to matrix stiffness in three-dimensional biopolymer networks. Acta Biomater. 2015;13:61–7.

137. Zhao R, Zhou X, Khan ES, Alansary D, Friedmann KS, Yang W, et al. Targeting the microtubule-network rescues CTL killing efficiency in dense 3D matrices. Front Immunol. 2021;12:729820.

138. Riedel S, Hietschold P, Krömmelbein C, Kunschmann T, Konieczny R, Knolle W, et al. Design of biomimetic collagen matrices by reagent-free electron beam induced crosslinking: structure-property relationships and cellular response. Mater Des. 2019;168:107606.

139. Adams G, López MP, Cartagena-Rivera AX, Waterman CM. Survey of cancer cell anatomy in nonadhesive confinement reveals a role for filamin-a and fascin-1 in leader bleb-based migration. Mol Biol Cell. 2021;32:1772–91.

140. Lavenus SB, Vosatka KW, Caruso AP, Ullo MF, Khan A, Logue JS. Emerin regulation of nuclear stiffness is required for fast amoeboid migration in confined environments. J Cell Sci. 2022;135:jcs259493.

141. Ullo MF, Logue JS. ADF and cofilin-1 collaborate to promote cortical actin flow and the leader bleb-based migration of confined cells. Elife. 2021;10:e67856.

142. Ruprecht V, Wieser S, Callan-Jones A, Smutny M, Morita H, Sako K, et al. Cortical contractility triggers a stochastic switch to fast amoeboid cell motility. Cell. 2015;160:673–85.

143. Sanz-Moreno V, Marshall CJ. The plasticity of cytoskeletal dynamics underlying neoplastic cell migration. Curr Opin Cell Biol. 2010;22:690–6.

144. Paluch EK, Raz E. The role and regulation of blebs in cell migration. Curr Opin Cell Biol. 2013;25:582–90.

145. Guzman A, Avard RC, Devanny AJ, Kweon OS, Kaufman LJ. Delineating the role of membrane blebs in a hybrid mode of cancer cell invasion in three-dimensional environments. J Cell Sci. 2020;133.

146. Huang B, Lu M, Jolly MK, Tsarfaty I, Onuchic J, Ben-Jacob E. The three-way switch operation of Rac1/RhoA GTPase-based circuit controlling amoeboid-hybrid-mesenchymal transition. Sci Rep. 2014;4:6449.

147. Gabbireddy SR, Vosatka KW, Chung AJ, Logue JS. Melanoma cells adopt features of both mesenchymal and amoeboid migration within confining channels. Sci Rep. 2021;11:17804.

148. Tolde O, Gandalovičová A, Křížová A, Veselý P, Chmelík R, Rosel D, et al. Quantitative phase imaging unravels new insight into dynamics of mesenchymal and amoeboid cancer cell invasion. Sci Rep. 2018;8:12020.

149. Brassart B, Da Silva J, Donet M, Seurat E, Hague F, Terryn C, et al. Tumour cell blebbing and extracellular vesicle shedding: key role of matrikines and ribosomal protein SA. Br J Cancer. 2019;120:453–65.

150. Kim J, Morley S, Le M, Bedoret D, Umetsu DT, Di Vizio D, et al. Enhanced shedding of extracellular vesicles from amoeboid prostate cancer cells:

potential effects on the tumor microenvironment. Cancer Biol Ther. 2014;15:409–18.

151. Rilla K. Diverse plasma membrane protrusions act as platforms for extracellular vesicle shedding. J Extracell vesicles. 2021;10:e12148.

152. Ciardiello C, Migliorino R, Leone A, Budillon A. Large extracellular vesicles: size matters in tumor progression. Cytokine Growth Factor Rev. 2020;51:69–74.

153. Di Vizio D, Morello M, Dudley AC, Schow PW, Adam RM, Morley S, et al. Large oncosomes in human prostate cancer tissues and in the circulation of mice with metastatic disease. Am J Pathol. 2012;181:1573–84.

154. Chrisafis G, Wang T, Moissoglu K, Gasparski AN, Ng Y, Weigert R, et al. Collective cancer cell invasion requires RNA accumulation at the invasive front. Proc Natl Acad Sci U S A. 2020;117:27423–34.

155. Abiri A, Lavigne M, Rezaei M, Nikzad S, Zare P, Mergny JL, et al. Unlocking G-quadruplexes as antiviral targets. Pharmacol Rev. 2021;73:897–923.

156. Ruggiero E, Zanin I, Terreri M, Richter SN. G-quadruplex targeting in the fight against viruses: an update. Int J Mol Sci. 2021;22:10984.

157. Sanchez-Martin V, Lopez-Pujante C, Soriano-Rodriguez M, Garcia-Salcedo JA. An updated focus on quadruplex structures as potential therapeutic targets in cancer. Int J Mol Sci. 2020;21:8900.

158. Awadasseid A, Ma X, Wu Y, Zhang W. G-quadruplex stabilization via small-molecules as a potential anti-cancer strategy. Biomed Pharmacother. 2021;139:111550.

159. Zhao C, Qin G, Niu J, Wang Z, Wang C, Insong Ren J, et al. Targeting RNA G-quadruplex in SARS-CoV-2: a promising therapeutic target for COVID-19? Angew Chem. 2021;133:436–42.

160. Hu XX, Wang SQ, Gan SQ, Liu L, Zhong MQ, Jia MH, et al. A small ligand that selectively binds to the G-quadruplex at the human vascular endothelial growth factor internal ribosomal entry site and represses the translation. Front Chem. 2021;9:960.

161. Pandya N, Khan E, Jain N, Satham L, Singh R, Makde RD, et al. Curcumin analogs exhibit anti-cancer activity by selectively targeting G-quadruplex forming c-myc promoter sequence. Biochimie. 2021;180:205–21.

162. Kozomara A, Birgaoanu M, Griffiths-Jones S. miRBase: from microRNA sequences to function. Nucleic Acids Res. 2019;47:D155–62.

163. Kikin O, D'Antonio L, Bagga PS. QGRS mapper: a web-based server for predicting G-quadruplexes in nucleotide sequences. Nucleic Acids Res. 2006;34(Web Server issue):W676–82.

164. Stark M, Wichman C, Avivi I, Assaraf YG. Aberrant splicing of folylpoly-glutamate synthetase as a novel mechanism of antifolate resistance in leukemia. Blood. 2009;113:4362–9.

165. Vera M, Tutucci E, Singer RH. Imaging single mRNA molecules in mammalian cells using an optimized MS2-MCP system. Methods Mol Biol. 2019;2038:3–20.

166. Wu B, Miskolci V, Sato H, Tutucci E, Kenworthy CA, Donnelly SK, et al. Synonymous modification results in high-fidelity gene expression of repetitive protein and nucleotide sequences. Genes Dev. 2015;29:876–86.

167. Lehvy AI, Horev G, Golan Y, Glaser F, Shammai Y, Assaraf YG. Alterations in ZnT1 expression and function lead to impaired intracellular zinc homeostasis in cancer. Cell Death Dis. 2019;5:1–12.

168. Subach OM, Cranfill PJ, Davidson MW, Verkhusha VV. An enhanced monomeric blue fluorescent protein with the high chemical stability of the chromophore. PLoS One. 2011;6:e28674.

Publisher's Note